Environ Monit Assess (2023) 195:944
https://doi.org/10.1007/s10661-023-11560-8

RESEARCH

Remote sensing environmental indicators for monitoring spatial and temporal dynamics of weather and vegetation conditions: applications for Brazilian biomes

Antônio Teixeira · Janice Leivas · Celina Takemura · Gustavo Bayma · Edlene Garçon · Inajá Sousa · Franzone Farias · Cesar Silva

Received: 4 March 2023 / Accepted: 26 June 2023

Abstract The SAFER (Simple Algorithm for Evapotranspiration Retrieving) algorithm and the radiation use efficiency (RUE) model were coupled to test large-scale remote sensing environmental indicators in Brazilian biomes. MODIS MOD13Q1 reflectance product and gridded weather data for the year 2016 were used to demonstrate the suitability of the algorithm to monitor the dynamics of environmental remote sensing indicators along a year in the Brazilian biomes, Amazon, Caatinga, Cerrado, Pantanal, Atlantic Forest, and Pampa. Significant spatial and temporal variations in precipitation (*P*), actual evapotranspiration (ET), and biomass production (BIO) yielded differences on water balance (WB = *P* − ET) and water productivity (WP = ET/BIO). The highest WB and WP differences were detected in the wettest biomes, Amazon, Atlantic Forest, and Pampa, when compared with the driest biome, Caatinga. Rainfall distribution along the year affected the magnitude of the evaporative fraction (ET_f), i.e., the ET to reference evapotranspiration (ET_0) ratio. However, there was a gap between ET_f and WB, which may be related to the time needed for recovering good soil moisture conditions after rainfalls. For some biomes, BIO related most to the levels of absorbed photosynthetically active radiation (Amazon and Atlantic Forest), while for others, BIO followed most the soil moisture levels, depicted by ET_f (Caatinga, Cerrado, Pantanal, and Pampa). The large-scale modeling showed suitability for monitoring the water and vegetation conditions, making way to detect anomalies for specific periods along the year by using historical images and weather data, with strong potential to support public policies for management and conservation of natural resources and with possibilities for replication of the methods in other countries.

A. Teixeira (✉)
Federal University of Sergipe (UFS), São Cristóvão, SE, Brazil
e-mail: heribertoteixeira11@gmail.com

J. Leivas · C. Takemura · E. Garçon
Embrapa Territory, Campinas, SP, Brazil
e-mail: janice.leivas@embrapa.br

C. Takemura
e-mail: celina.takemura@embrapa.br

E. Garçon
e-mail: edlene.garcon@embrapa.br

G. Bayma
Embrapa Environment, Jaguariuna, SP, Brazil
e-mail: gustavo.bayma@embrapa.br

I. Sousa · F. Farias
Federal University of Sergipe (UFS), São Cristóvão, SE, Brazil
e-mail: inajafrancisco@gmail.com

F. Farias
e-mail: franzone.farias@hotmail.com

C. Silva
University of Campinas (UNICAMP), Campinas, SP, Brazil
e-mail: cesaroliveira.f.silva@gmail.com

Published online: 12 July 2023

Keywords Precipitation · Evapotranspiration · Water balance · Biomass production · Water productivity

Introduction

In several places of the world, water demands and population are growing under unsustainable natural resource consumption. The consequent environmental impacts have been generally measured on local scales; however, with continuous development of remote sensing technologies, they can nowadays be analyzed using environmental indicators on a country scale with acceptable accuracies. Under climate and land-use change scenarios, these technologies are powerful tools to monitor the effects of these changes, what should be considered when aiming at sustainable development (de Teixeira, Leivas, et al., 2020; de Teixeira, Leivas, Pacheco, et al., 2021; de Teixeira, Leivas, Struiving, et al., 2021; de Teixeira, Takemura, et al., 2020; Jardim et al., 2022).

Climate and land-use changes affect energy, water, and carbon balances (Ceschia et al., 2010; Zhao & Running, 2010). Understanding the responses of water and vegetation parameters and their dynamics is critical for ecological restoration and for assessments of these balances (Yang et al., 2016; Zhang & Zhang, 2019). Brazilian biomes feature a large diversity of natural species (Lewinsohn & Prado, 2005) and suffer under several environmental impacts, such as deforestation, burnings, air, water, and soil pollution, as well as intensive agricultural crops replacing natural species (Casagrande et al., 2021; Mariano et al., 2018). These problems demand large-scale studies to support sustainable consumptions of the natural resources (Araujo et al., 2019; de Teixeira, Leivas, Pacheco, et al., 2021; de Teixeira, Leivas, Struiving, et al., 2021; Jardim et al., 2022; Nuñez et al., 2017; Santos et al., 2020).

Quantifying energy, water, and carbon balance components by using remote sensing together with gridded weather data in mixed agroecosystems is a suitable way to elaborate and apply environmental indicators to support the rational management of natural resources. After accounting for all the radiation balance components, the net radiation (R_n) is the difference between incoming and outgoing radiation for both short and long wavelengths, and R_n is partitioned into latent (λE), sensible (H), and ground (G) heat fluxes. Acquiring λE deserves highlighting, because it represents the energy for actual evapotranspiration—ET, which is the main use of water resources by well-watered vegetation and is also related to biomass production—BIO (de Teixeira, Leivas, et al., 2020; de Teixeira, Takemura, et al., 2020).

On the one hand, although ET is related to BIO, increasing its rates means less water availability for ecological and human uses. On the other hand, H magnitude may indicate surface warming or cooling effects (Bhattarai et al., 2017; de Teixeira, Leivas, et al., 2020; de Teixeira, Leivas, Struiving, et al., 2021). Regarding carbon balance, replacing natural vegetation with agricultural crops may produce carbon sinks, affecting BIO (Ceschia et al., 2010), while water scarcity increases vegetation mortality rates and changes the ecosystem's species compositions (Zhao & Running, 2010). Quantifying these effects and monitoring their dynamics along the years is essential for ecological restoration and to assess the dimension of environmental impacts (Yang et al., 2016; Zhang & Zhang, 2019).

Some energy, water, and carbon balance field measurements have been done using different methods in distinct Brazilian agroecosystems (Cabral et al., 2015; da Silva et al., 2017; de Teixeira et al., 2008; Lathuillière et al., 2018; Marin et al., 2019; Marques et al., 2020; Rubert et al., 2018). However, few efforts have been carried out to produce environmental indicators for comparisons among the different biomes along the country. In addition, point measurements are not suitable for these comparisons, because of large spatial variations of weather and climate conditions within the biomes. Due to these limitations, up-scaling environmental indicators by means of remote sensing algorithms is a suitable alternative to support environmental policies.

Due to its operational characteristic while maintaining the physical basis, the Penman-Monteith equation has been suggested for coupling remote-sensing parameters and weather data (Cleugh et al., 2007; Consoli et al., 2016; Consoli & Vanella, 2014; Nagler et al., 2013; Olivera-Guerra et al., 2018). When applied together with gridded weather data, this equation has potential for use with low spatial resolution satellite images (Mateos et al., 2013; Vanella et al., 2019). Considering the operationality of the Penman-Monteith equation for large-scale

applications, the SAFER (Simple Algorithm for Evapotranspiration Retrieving) algorithm was developed using simultaneous field and remote-sensing measurements in irrigated crops and natural vegetation under strong thermohydrological conditions in the Brazilian Northeast region, to determine environmental remote-sensing based indicators (de Teixeira, 2010; de Teixeira et al., 2008).

Besides its applicability, the actual version of SAFER does not require the use of satellite thermal bands to estimate ET. This one of the main reasons why it was chosen in the current research, because by using the MODIS thermal band, the spatial resolution of 1 km implies that the images will cover more pixels containing mixed land-cover types. Coupling the SAFER algorithm with Monteith's radiation use efficiency (RUE) model (Monteith, 1977) to estimate BIO has great potential for environmental studies under climate and land-use changes conditions (de Teixeira, Leivas, et al., 2020; de Teixeira, Takemura, et al., 2020; de Teixeira, Leivas, Pacheco, et al., 2021). The remote-sensing parameters considered in the current paper to elaborate and test the environmental indicators are combinations of ET and BIO with gridded on precipitation (*P*) data, retrieving the water balance and water productivity components.

The RUE model, based on absorbed photosynthetically active radiation, may be used inside remote-sensing algorithms to retrieve BIO on a country scale (Bastiaanssen & Ali, 2003; Claverie et al., 2012; Franco et al., 2016; Nyolei et al., 2019; Rampazo et al., 2020; de Teixeira et al., 2018; de Teixeira, Leivas, Pacheco, et al., 2021; Zhao et al., 2005). The BIO to ET ratio, i.e., water productivity (WP), is another important environmental indicator, which may aid with sustainable managements of natural resources on different spatial and temporal scales (Franco et al., 2016; Nyolei et al., 2019; de Teixeira, Leivas, Pacheco, et al., 2021). Improving WP decreases the additional water used in agriculture, resulting in more water resources available for the maintenance of ecosystems (Molden et al., 2007), an important issue in biomes where natural vegetation is being intensively replaced by agricultural crops.

Aiming at the operational implementation of country-scale monitoring system that uses historical data sets, and using Brazil as reference, we tested the latest version of the SAFER algorithm together with Monteith's RUE model. We used MODIS' MOD13Q1 reflectance product and 16-day weather data for the year 2016. This was done to demonstrate the suitability of the algorithm' application to monitor dynamics of environmental remote sensing indicators derived from energy, water, and carbon balance components in distinct biomes. The reasons for using data from 2016 are twofold: Brazilian ecosystems were recovering their good levels of soil moisture, after a prolonged drought period from 2012 to 2015 (Mariano et al., 2018; Rebello et al., 2020), and the availability weather data covering the whole country during this year. The spatial determinations of ET and BIO and their association with precipitation gridded data will be useful to subsidize public policies regarding the management and conservation of the natural resources. Although the modeling was tested for only one year, historical series of data may be used to detect anomalies for specific periods of any year. The successful applications carried out of this scientific research in Brazil may encourage replications of the methods in other countries through simple calibrations of the modeling equations.

Material and methods

Biomes and data set

Figure 1 presents the locations of the 491 weather stations used from the Brazilian National Institute of Meteorology (INMET - https://www.gov.br/agricultura/pt-br/assuntos/inmet) and highlights Brazilian geographic regions with their altitudes and biomes, classified according to the Brazilian Institute of Geographic and Statistics (IBGE - www.ibge.gov.br).

The Amazon biome has tropical rainforest climate with high air temperatures (Casagrande et al., 2021; Nobre et al., 2016); Caatinga and Cerrado face frequent droughts, and their natural species develop resilience with increasing aridity under these dry conditions (Almagro et al., 2017; de Azevedo et al., 2020; Jardim et al., 2022; Sano et al., 2019; Santos et al., 2014); Pantanal is the largest tropical wetland in the world, with two well-defined seasons: a rainy summer and a dry winter (Assine et al., 2015; Marengo et al., 2021); Atlantic Forest has a humid tropical climate (Ribeiro et al., 2009), but contrasting microclimates among natural and anthropized areas (Souza Jr et al., 2020);

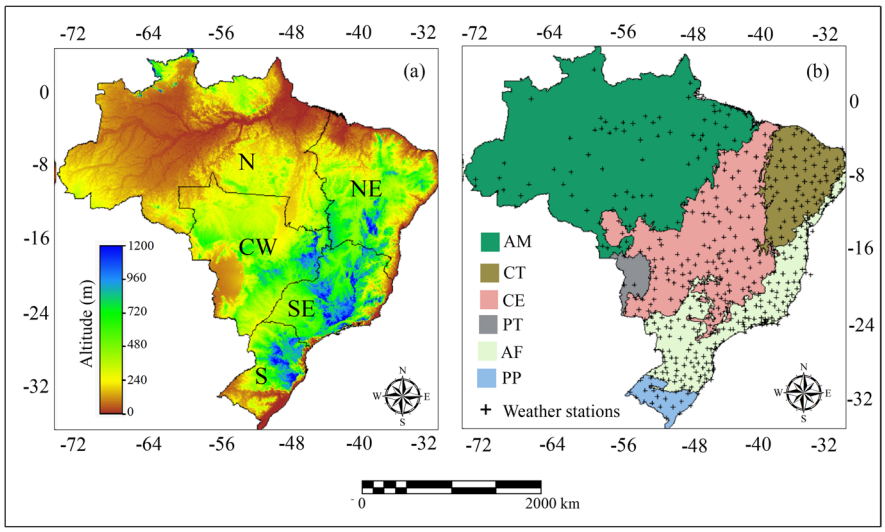

Fig. 1 Brazilian geographic regions, altitudes, biomes, and weather stations used with remote-sensing parameters. Geographic regions: N, North; NE, Northeast; CW, Central West; SE, Southeast; S, South (**a**). Biomes: AM, Amazon; CT, Caatinga; CE, Cerrado; PT, Pantanal; AF, Atlantic Forest; PP, Pampa (**b**)

and Pampa has temperate climate with low air temperatures (Roesch et al., 2009; Rubert et al., 2018).

The weather data obtained from the Brazilian National Institute of Meteorology (INMET) were interpolated using the geostatistical "moving average" method and used for the reference evapotranspiration (ET_0) calculations, by applying the Penman-Monteith method (Allen et al., 1998). These gridded data were coupled with reflectance pixel values from bands 1 and 2 of MODIS' MOD13Q1 product, at a spatial resolution of 250 m and temporal resolution of 16 days, downloaded from the EARTHDATA AppEEARS' site (https://lpdaacsvc.cr.usgs.gov/appeears/), to derive the large-scale environmental indicators. Despite low densities of stations in some places, such as the Amazon biome, their interpolated weather data resampled to the MODIS image resolution had enough accuracy for better characterization of the spatial weather conditions. For quarter (Q) analyses, the average MODIS 16-day images and up-scaled daily weather data for this temporal scale were considered between January and March ($Q1$), April and June ($Q2$), July and September ($Q3$), and October to December ($Q4$). For water balance (WP), total precipitation (P) within these periods was used together with total ET, taking the average daily ET value and the number of days for these quarters.

Remote sensing environmental indicators modeling

Figure 2 shows the flowchart for modeling the large-scale remote sensing environmental indicators by applying the SAFER algorithm and the RUE model using MODIS' MOD13Q1 reflectance product and gridded weather data.

All regression coefficients described in Fig. 2 were previously determined and statistically validated by simultaneous satellite and field measurements made in Northeast Brazil (de Teixeira, 2010; de Teixeira et al., 2008; de Teixeira et al., 2013). The field data used involved irrigated crops and natural vegetation (Caatinga) from 2001–2007 with strong thermos-hydrological and soil cover contrasts, collected in irrigated crops and natural vegetation (Caatinga) from 2001 to 2007. Table grapes were micro-sprinkler irrigated and conducted by an overhead trellis system, wine grapes were drip irrigated and conducted by a vertical trellis system, and mango orchard were micro sprinkler irrigated. The experimental period for Caatinga involved different species and rainfall conditions above and below the local long-term value (de Teixeira et al., 2008).

In the current paper, a correction factor is applied to the evaporative fraction (ET_f) in the main SAFER's equation, to consider distinct atmospheric demands for ET acquirements regarding the original modeling conditions. Thus, the SAFER algorithm has been validated in several Brazilian agroecosystems (Araujo et al., 2019; Leivas et al., 2015; Nuñez et al., 2017; Rampazo et al., 2020; Santos et al., 2020; Silva et al., 2019; de Teixeira, Leivas, et al., 2020; de Teixeira, Takemura, et al., 2020; de Teixeira, Leivas, Struiving, et al., 2021; de Teixeira, Leivas, Pacheco, et al., 2021; Venancio et al., 2021). Besides these previous validations, the corrected ET_f values were satisfactorily checked

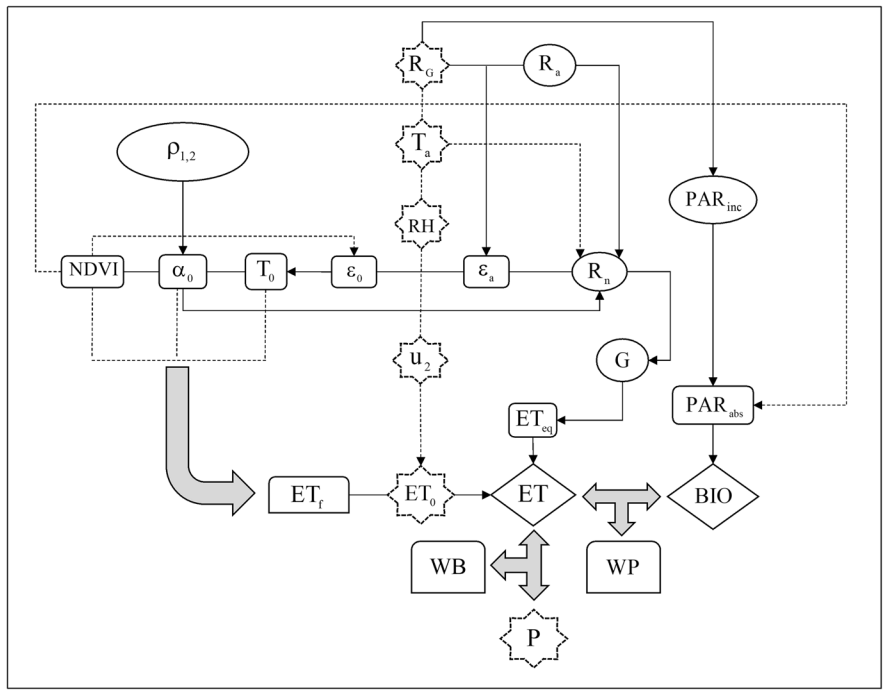

Fig. 2 Flowchart for modeling the large-scale remote sensing environmental indicators, by using the MODIS MO13Q1 reflectance product, together with gridded weather data. Dashed polygonal shaped boxes are data from the weather stations. Note: $\rho_{1,2}$, reflectance from bands 1 and 2, respectively; NDVI, normalized difference vegetation index; α_0, surface albedo; T_0, surface temperature; R_G, incident global solar radiation at the surface; R_a, incident solar radiation at the top of the atmosphere; T_a, air temperature; *RH*, relative humidity; u_2, wind speed at 2-m height; ET_f, evapotranspiration fraction; ET_0, reference evapotranspiration; ε_0, surface emissivity; ε_a, atmospheric emissivity; R_n, net radiation; G, ground heat flux; ET_{eq}, equilibrium evapotranspiration; ET, actual evapotranspiration; P, precipitation; WB, water balance; PAR_{inc}, incident photosynthetically active radiation; PAR_{abs}, absorbed photosynthetically active radiation; BIO, biomass production; WP, water productivity

against those from literature, as well. Thus, one may expect sufficient accuracy for our main objective of testing an operational monitoring system for environmental indicators, allowing comparisons among biomes, and offering a first insight into their spatial and temporal dynamics. To attain this goal, new expensive validations with simultaneous field and satellite data are not strictly necessary, since they are very difficult and expensive for many local conditions in Brazil, along the years.

Following Fig. 2, the α_0 pixel values were calculated as

$$\alpha_0 = a + b\rho_1 + c\rho_2 \tag{1}$$

where ρ_1 and ρ_2 are the MODIS reflectances from bands 1 (red) and 2 (near infra-red), respectively; a, b, and c are regression coefficients (Araujo et al., 2019; Rampazo et al., 2020). In the Northeast region of Brazil, coefficients a, b, and c were 0.08, 0.41, and 0.14, and involved irrigated crops and natural vegetation under contrasting thermo-hydrological conditions may be calibrated for specific environments if more accuracy for α_0 is desirable (de Teixeira et al., 2008, de Teixeira et al., 2013).

NDVI is used as a remote-sensing parameter for surface cover and moisture conditions:

$$NDVI = \frac{\rho_2 - \rho_1}{\rho_2 + \rho_1} \tag{2}$$

With R_G and T_a measured at the weather stations, and R_a astronomically calculated, R_n was estimated using the Slob equation (de Bruin, 1987):

$$R_n = \left(1 - \alpha_0\right)R_G - a_L\tau_{sw} \tag{3}$$

where τ_{sw} is the short-wave atmospheric transmissivity (R_G/R_a) and a_L is a regression coefficient up-scaled throughout the T_a pixel values.

$$a_L = a_T T_a + b_T \tag{4}$$

where the regression coefficients a_T and b_T for the Northeast region, involving strong thermos-hydrological conditions, were 6.8 and −40, respectively, but may be adjusted for specific environmental conditions (de Teixeira, 2010; de Teixeira et al., 2008).

The atmospheric emissivity (ε_A) was calculated according to de Teixeira, Leivas, Struiving, et al. (2021); de Teixeira, Leivas, Pacheco, et al. (2021):

$$\varepsilon_A = a_A \left(\ln \tau_{sw}\right)^{b_A} \tag{5}$$

where a_A and b_A are regression coefficients, which are reported as 0.94 and 0.11, respectively, for the Northeast region, involving strong thermo-hydrological conditions, but may be calibrated using field radiation balance measurements for specific environmental environments (de Teixeira, 2010; de Teixeira et al., 2008).

Surface emissivity (ε_0) was estimated according to Rampazo et al. (2020) and Silva et al. (2019):

$$\varepsilon_0 = a_0 \ln NDVI + b_0 \tag{6}$$

where a_0 and b_0 are regression coefficients, which were reported as 0.06 and 1.00 for the Northeast region, involving strong thermos-hydrological conditions, but may be acquired for specific environmental environments by simultaneous field radiation balance and remote sensing NDVI measurements (de Teixeira, 2010; de Teixeira et al., 2008).

Using the residual method, according to the physical principle of the Stefan-Boltzmann' low, T_0 was estimated as (Rampazo et al., 2020; Silva et al., 2019)

$$T_0 = \frac{\sqrt[4]{R_G\left(1-\alpha_0\right) + \sigma\varepsilon_a {T_a}^4 - R_n}}{\sigma\varepsilon_0} \tag{7}$$

where $\sigma = 5.67\ 10^{-8}$ W m^{-2} K^{-4} is the Stefan-Boltzmann constant.

To acquire ET, its ratio to ET_0 (the evapotranspiration fraction - ET_f) was modeled (Araujo et al., 2019; Dehziari & Sanaienejad, 2019; Venancio et al., 2021):

$$ET_f = \exp\left[a_{sf} + b_{sf}\left(\frac{T_0}{\alpha_0 NDVI}\right)\right]\frac{ET_{0_{year}}}{5} \tag{8}$$

where a_{sf} and b_{sf} are regression coefficients for the Northeast region valued 1.90 and −0.008, being possible to be calibrated using field measurements for ET and ET_0 and the remote-sensing parameters α_0, NDVI, and T_0 in contrasting hydrological surfaces (Venancio et al., 2021; de Teixeira, Leivas, Pacheco, et al., 2021; Safre et al., 2022; de Almeida, Souza, Nogueira, et al., 2023; de Almeida, Souza, Pilon, et al., 2023). As these measurements are very difficult and expensive in the whole Brazil, we introduced $\frac{ET_{0_{year}}}{5}$ as a correction factor to consider distinct atmospheric demands regarding the original modeling region, with the denominator of 5 mm d^{-1} being the annual reference evapotranspiration ($ET_{0_{year}}$) for the period when the SAFER algorithm was elaborated in the Brazilian Northeast (de Teixeira, 2010; de Teixeira et al., 2008), as the same weather parameters affecting ET_0 will also affect ET.

Equation 8 does not work for water bodies or mixtures of land and water (NDVI <0); thus, under these circumstances, the concept of equilibrium evapotranspiration—ET_{eq} (Raupasch, 2001) —is used in the SAFER algorithm:

$$ET_{eq} = 0.035\left(\frac{\Delta\left(R_n - G\right)}{\Delta + \gamma}\right) \tag{9}$$

where Δ is the inclination of the curve relating the saturation vapor pressure (e_s) and T_a, γ is the psychrometric constant, and G is estimated according to

$$\frac{G}{R_n} = a_G \exp\left(b_G \alpha_0\right) \tag{10}$$

where a_G and b_G are regression coefficients, 3.98 and −25.47, respectively, for the Northeast region, involving strong thermos-hydrological conditions, but may be calibrated using simultaneous field energy balance measurements for other environmental conditions (de Teixeira, 2010; de Teixeira et al., 2008).

Throughout conditional functions applied to the NDVI values, daily ET pixel values were acquired as

$$ET = ET_f ET_0 \ or \ ET_{eq} \tag{11}$$

where ET_0 was calculated using daily gridded weather data on R_G, T_a, RH, and u_2 (de Teixeira, Leivas, et al., 2020; de Teixeira, Takemura, et al., 2020).

Similarly, to what was done in Australia (Cleugh et al., 2007) and Southeast Brazil (de Teixeira et al., 2017), water balance (WB) was computed as

$$WB = P - ET \tag{12}$$

where P are gridded precipitation data from the net of weather stations.

For BIO large-scale estimations, Monteith's RUE model (Monteith, 1977) was applied introducing the root-zone moisture effect through ET_f (Araujo et al., 2019; Franco et al., 2016; Nuñez et al., 2017; Rampazo et al., 2020; de Teixeira et al., 2018; de Teixeira, Leivas, Pacheco, et al., 2021; de Almeida, Souza, Nogueira, et al., 2023; de Almeida, Souza, Pilon, et al., 2023):

$$BIO = \varepsilon_{\max} ET_f PAR_{abs} 0.864 \tag{13}$$

where $\varepsilon_{\max}$ is the maximum radiation efficiency use, which for the majority of C3 crops in Brazilian biomes was considered 2.45 g MJ^{-1} (Bastiaanssen & Ali, 2003); and 0.864 is the unit conversion factor.

According to Monteith (1972), if not under water stressed, $\varepsilon_{\max}$ varies only if the crops are C3 and C4. The improvements to Monteith's model have resulted in corrections for environmental conditions, including soil moisture and heat stresses. However, even though some uncertainties about the $\varepsilon_{\max}$ values arise, due to spatiotemporal variations (van Heerden et al., 2010; Zhao et al., 2005) and moisture conditions (de Silva & De Costa, 2012), a constant value has been considered acceptable for large-scale remote-sensing applications (Bastiaanssen & Ali, 2003; Franco et al., 2016; Nuñez et al., 2017; Nyolei et al., 2019; de Teixeira, Leivas, et al., 2020; de Teixeira, Takemura, et al., 2020; Zwart et al., 2010). Considering the strong biodiversity of the whole Brazil and our objective of having a monitoring system to offer a first insight into water and vegetation conditions for further detailed observations, considering the majority of C3 species has enough accuracy for our purpose, overcoming the lack of expensive observations over the whole country.

PAR_{abs} was estimated from PAR_{inc}, which in turn was considered as a fraction of R_G:

$$PAR_{abs} = \left(a_p NDVI + b_p\right) PAR_{inc} \tag{14}$$

where a_p and b_p are regression coefficients, 1.257 and −0,161, respectively, found in mixed crops (Bastiaanssen & Ali, 2003), but they may be calibrated for specific environmental conditions using field measurements of PAR_{inc} and PAR_{abs} together with NDVI values.

Water productivity (WP) was considered as (de Teixeira, Leivas, Pacheco, et al., 2021):

$$WP = \frac{BIO}{ET} \tag{15}$$

Analysis of variance (ANOVA) was performed using 2-way ANOVA in R (ver. 3.5.1) with a pairwise comparison by applying the Tuckey honestly significant difference (HSD) post hoc test at the 5% significance level, for the six Brazilian biomes at quarter and annual timescales. HSD is an integral part of ANOVA to test the equality of at least three group means. Statistically significant results indicate that not all the group means are equal, exploring differences between them while controlling the wise error rates.

Results and discussions

Water balance dynamics

Figure 3 shows the spatial distributions of the quarterly average totals for precipitation (P), together with the mean pixel values and standard deviations (SD), for each Brazilian geographic region, along the year 2016.

Spatial and temporal variations on P pixel values along the year are strongly noticed among quarters and geographic regions. The lowest values were detected in the Northeast ($Q4$), where the Caatinga biome is concentrated, and the highest ones in the North ($Q1$), with only the Amazon biome (see also Fig. 1). Intercrossing Figs. 1b and 3, Table 1 presents the quarterly and annually average totals of P and standard deviation (SD) values, for each of Brazilian biome during the year 2016, together with the pairwise comparisons from Tuckey's honestly significant difference (HSD) post hoc test.

According to Tuckey's HSD post hoc test, significant differences on P values arise among biomes. The highest values were detected for Amazon and Pampa, during all quarters of the year, and from April

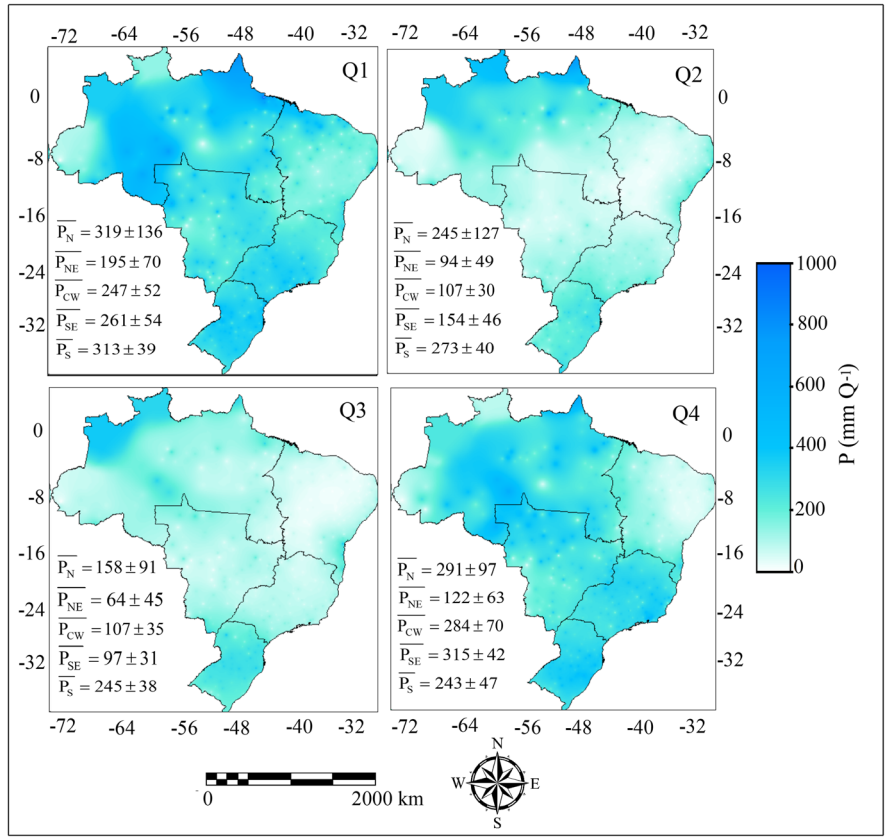

Fig. 3 Spatial distributions of the quarterly average precipitation (*P*) values for each Brazilian geographic regions, together with the averages and standard deviations (SD) during 2016. Overlines mean the average *P* total for the region. Quarters (*Q*): *Q*1—January to March, *Q*2—April to June, *Q*3—July to September, and *Q*4—October to December. Geographic regions: North—N, Northeast—NE, Central West—CW, Southeast—SE, and South—S

Table 1 Quarterly and annually average total values of precipitation (*P*) and standard deviations (SD) for each Brazilian biome, during the year 2016, together with the pairwise comparisons from Tuckey's honestly significant difference (HSD) post hoc test

Quarter[1]/biome[2]	*Q*1 (mm Q^{-1})	*Q*2 (mm Q^{-1})	*Q*3 (mm Q^{-1})	*Q*4 (mm Q^{-1})	Year (mm yr^{-1})
AM	319 ± 130c	236 ± 124c	157 ± 86c	297 ± 98c	1,009 ± 320c
CT	174 ± 52a	82 ± 38a	50 ± 29a	84 ± 44a	390 ± 93a
CE	233 ± 55b	102 ± 39a	83 ± 31a	255 ± 68b	672 ± 153b
PT	202 ± 39a	96 ± 22a	85 ± 18a	195 ± 37a	578 ± 91a
AF	275 ± 62b	211 ± 62b	170 ± 80b	300 ± 82b	956 ± 230b
PP	298 ± 34c	265 ± 41c	226 ± 29c	346 ± 42c	1,135 ± 112c
Mean	250 ± 62	165 ± 54	128 ± 46	246 ± 62	789 ± 167

[1]Quarters (*Q*): *Q*1—January to March, *Q*2—April to June, *Q*3—July to September, and Q4—October to December. [2]Biomes: AM—Amazon, CT—Caatinga, CE—Cerrado, PT—Pantanal, AF—Atlantic Forest, and PP—Pampa. *P* values with the same letter in each column indicate no significant differences from each other at 5% (pairwise comparisons using Tuckey's HSD post hoc test for each quarter and for the whole year)

to September (*Q*2 to *Q*3) for Cerrado; while for Pantanal, from January to December (*Q*1 to *Q*4), there were no significant differences, in comparison with the driest Caatinga biome.

In Amazon, with an annual *P* of 1,009 mm yr^{-1}, the highest quarterly rainfall amounts occurred in *Q*1 (January to March), with average total above 315 mm Q^{-1}. The lowest values happened in *Q*3 (July

to September), when the average total was below 160 mm Q^{-1}, but showing the highest spatial variations among quarters, with standard deviation (SD) accounting for 55% of the average. The lowest SD occurred in *Q*4 (October to December) when it represented 33% of the mean total value. In central Amazon, Kunert et al. (2017) reported a higher annual rainfall of 2,302 mm in 2013, but drier conditions in 2016 were detected in 2016 for this biome in the current study.

Among the Brazilian biomes, Caatinga showed the lowest rainfall amounts, with an annual *P* around 390 mm yr^{-1}. The smallest average quarterly value was 50 mm Q^{-1}, during *Q*3 (July to September), when happened the highest spatial variations, with SD accounting for 58% of the average. However, during the rainy period, the mean total was above 170 mm Q^{-1} in *Q*1 (January to March), when occurred the lowest SD, accounting for 30% of the average. da Silva et al. (2017) reported an annual *P* of 430 mm in the Caatinga from 2014 to 2015, a little higher than our value in Table 1, showing that this biome suffered much water scarcity along the year 2016.

The Cerrado biome showed an annual average *P* of 672 mm yr^{-1}, within the values from 560 to 1,663 mm yr^{-1} reported by Fernandes et al. (2018) for 2003 to 2014, but much lower than the highest end of this range. The largest rainfall amounts for this biome happened in *Q*4 (October to December), when the mean pixel total value was 255 mm Q^{-1} and the lowest values, below 85 mm Q^{-1}, were in *Q*3 (July to September). The highest and the smallest spatial variations occurred in *Q*2 (April to June) and *Q*1 (January to March), when SD represented 38 and 24% of the average, respectively.

In the Pantanal biome, with an annual average value of 578 mm yr^{-1}, the highest rates were detected in *Q*1 (January to March), when the mean *P* total was above 200 mm Q^{-1}. The lowest ones occurred in *Q*3 (July to September), around 85 mm Q^{-1}. The largest spatial variations happened in *Q*2 (April to June), when SD accounted for 23% of the mean pixel value, while the smallest ones were in *Q*1 (January to March), when SD accounted for 19% of the average. Moreira et al. (2019) reported an annual average *P* of 1,112 mm yr^{-1} based on measurements from 2003 to 2014, evidencing that this biome was climatically drier in 2016, when half of this value was detected in the current study.

For the Atlantic Forest biome, with an annual average *P* of 956 mm yr^{-1}, the highest quarterly value of 300 mm Q^{-1} occurred in *Q*4 (October to December), while the lowest one, 170 mm Q^{-1} happened in *Q*3 (July to September), when there were the largest spatial variations, with SD accounting for 47% of the mean pixel value. The lowest SD occurred in *Q*1 (January to March), when it was 23% of the average. Based on water balance measurements taking during the year 2008 in this biome, Pereira et al. (2010) reported an annual *P* of 1,313 mm yr^{-1}, a little higher than the value in Table 1.

The highest rainfall amounts among biomes happened for Pampa, with an annual average *P* value of 1,135 mm yr^{-1}. This biome showed the most regular rainfall distribution along the year when compared with the other ones and the highest *P* in *Q*4 (October to December), with an average total above 345 mm Q^{-1} and the lowest ones in Q3 (July to September), but still higher than 225 mm Q^{-1}. The slightly largest spatial variations were detected in *Q*2 (April to June), when SD accounted for only 11% of the average. Scottá and da Fonseca (2015) reported an annual average *P* for the Pampa biome of 1,446 mm yr^{-1}, a little higher than our annual value.

Considering all Brazilian biomes, the quarterly periods with the highest rainfall amounts were from January to March (*Q*1) in Amazon, Caatinga, and Pantanal; and from October to December (Q4) in Cerrado, Atlantic Forest, and Pampa. However, the lowest rainfall amounts for all of them were in *Q*3 (July to September). Comparing our precipitation values with literature data for all biomes, one may notice that during the year 2016, although vegetation was recovering from a drought period between 2012 and 2015 (Mariano et al., 2018; Rebello et al., 2020), rainfall amounts were still low.

Figure 4 shows the spatial distributions of the quarterly daily average actual evapotranspiration (ET), together with the mean pixel values and standard deviations (SD) for each Brazilian geographic region along the year 2016.

As for precipitation (*P*), spatial and temporal variations on ET pixel values among quarters and geographic regions are also strong, with the lowest values in the Northeast (*Q*3) where the Caatinga biome is concentrated and the highest ones in the South (*Q*3), with only the Pampa biome (see also Fig. 1). Intercrossing Figs. 1b and 4, Table 2 shows the quarterly

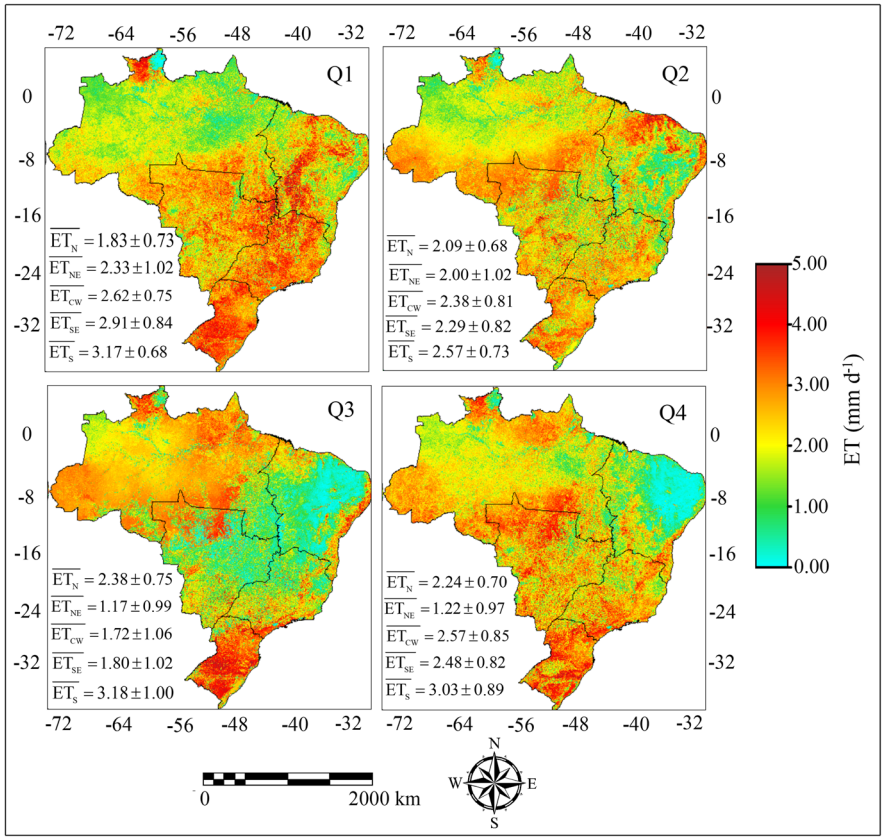

Fig. 4 Spatial distributions of the quarterly average actual evapotranspiration (ET) for each Brazilian geographic region, together with the mean pixel values and standard deviations (SD) during 2016. Overlines mean the average ET for the region. Quarters (*Q*): *Q*1—January to March, *Q*2—April to June, *Q*3—July to September, and *Q*4—October to December. Geographic regions: North—N, Northeast—NE, Central West—CW, Southeast—SE, and South—S

and annually average values of ET and standard deviations (SD) for each Brazilian biome during the year 2016, together with the pairwise comparisons from Tuckey's honestly significant difference (HSD) post hoc test.

According to Tuckey's HSD post hoc test, significant differences in ET rates were found among biomes; however, lower than those for precipitation (*P*), and the highest ones for the Pampa biome during *Q*1 (January to March), *Q*3 (July to September), and

Table 2 Quarterly and annually average values of actual evapotranspiration (ET) and standard deviations (SD) for each Brazilian biome during the year 2016, together with the pairwise comparisons from Tuckey's honestly significant difference (HSD) post hoc test

Quarter[1]/biome[2]	*Q*1 (mm d^{-1})	*Q*2 (mm d^{-1})	*Q*3 (mm d^{-1})	*Q*4 (mm d^{-1})	Year (mm d^{-1})
AM	1.89 ± 0.75a	2.17 ± 0.70a	2.44 ± 0.74b	2.31 ± 0.73b	2.20 ± 0.73b
CT	2.37 ± 1.00a	1.85 ± 1.08a	0.80 ± 0.83a	0.75 ± 0.79a	1.44 ± 0.93a
CE	2.66 ± 0.91a	2.18 ± 0.88a	1.33 ± 0.90a	2.21 ± 0.89b	2.10 ± 0.90b
PT	2.21 ± 0.79a	2.33 ± 0.67a	1.94 ± 0.79a	2.42 ± 0.88b	2.23 ± 0.78b
AF	2.84 ± 0.83b	2.41 ± 0.78b	2.49 ± 1.13b	2.68 ± 0.92b	2.61 ± 0.92b
PP	3.24 ± 0.71c	2.57 ± 0.81b	3.22 ± 1.01c	2.97 ± 0.97c	3.00 ± 0.98c
Mean	2.54 ± 0.83	2.25 ± 0.82	2.04 ± 0.90	2.22 ± 0.86	2.26 ± 0.85

[1]Quarters (*Q*): *Q*1—January to March, *Q*2—April to June, *Q*3—July to September, and *Q*4—October to December. [2]Biomes: AM—Amazon, CT—Caatinga, CE—Cerrado, PT—Pantanal, AF—Atlantic Forest, and PP—Pampa. ET rates with the same letter in each column indicate no significant differences from each other at 5% (pairwise comparisons using Tuckey's HSD post hoc test for each quarter and for the whole year)

*Q*4 (October to December); but there were no significant differences from January to June (*Q*1 to *Q*2) for Amazon and from January to September (*Q*1 to *Q*3) for Cerrado and Pantanal, when compared with the driest Caatinga biome.

For the Amazon biome, the highest ET rates occurred in *Q*3 (July to September), with a mean value above 2.40 mm d^{-1}, while the lowest ones were in *Q*1 (January to March), when the average was below 1.90 mm d^{-1}. On the annual scale, ET for this biome was 806 mm yr^{-1}. In Central Amazon, from eddy covariance measurements made in 2013, Kunert et al. (2017) reported a higher annual ET of 1,360 mm yr^{-1}. Casagrande et al. (2021) applied water balance models and found also higher annual ET values between 1,300 and 1,500 mm yr^{-1} in the Amazon Forest, using data from 2005 to 2015.

The Caatinga biome stands out for its strong hydrological contrast among quarters, with average ET below 0.80 mm d^{-1} during the driest conditions from July to December (*Q*3 to *Q*4), but above 2.30 mm d^{-1} within the rainiest period in *Q*1 (January to March). On the annual scale, it showed the lowest ET among biomes, with a mean total of 527 mm yr^{-1}. From eddy covariance measurements taken between 2014 and 2015 in this biome, da Silva et al. (2017) found average ET values from 0.98 mm d^{-1} during the dry season to 1.96 mm d^{-1} within the rainy season in this biome. Using the same energy balance techniques, also for the period from 2014 to 2015 in Caatinga, Marques et al. (2020) reported an average ET range between 0.20 and 0.30 mm d^{-1} during the dry season to values from 2.60 to 1.70 mm d^{-1} during the wet season. These rates are like the ones in Table 2.

In the Cerrado biome, the ET peaks were in *Q*1 (January to March), with average above 2.60 mm d^{-1}, while the lowest rates, below 1.40 mm d^{-1}, happened in *Q*3 (July to September). The annual ET of 767 mm yr^{-1} was a little lower than that for the Amazon. From eddy covariance measurements taken in Cerrado, Giambelluca et al. (2009) reported an average ET ranging from 1.91 to 2.25 mm d^{-1} and varying according to plant densities, while applying the SEBAL algorithm to Landsat images also in this biome, Laipelt et al. (2020) found average ET in grassland/pasture and agricultural areas between 2.0 and 3.2 mm d^{-1}. Both ranges from these studies involve our ET rates depicted in Table 2.

Regarding the Pantanal biome, the highest ET rates were detected in *Q*4 (October to December), when the average was above 2.40 mm d^{-1}, while the lowest ones occurred in *Q*3 (July to September), when it was below 2.00 mm d^{-1}. On the annual scale, ET for Pantanal was 814 mm yr^{-1}. From Bowen ratio measurements taken for different tree species within this biome, Sanches et al. (2011) reported average ET values of 2.50 and 4.00 mm d^{-1} for its dry and wet seasons, respectively. These rates are higher than those found in the current research, but specific for their studied ecosystems. However, using water balance measurements taken in the Pantanal biome, Moreira et al. (2019) found ET ranging between 1.63 and 3.53 mm d^{-1}, for the driest and rainiest periods, respectively. Considering the average values and standard deviations in Table 2, these last values are comparable.

For Atlantic Forest, the ET rates were more constant throughout the year than those detected for the previous biomes, with averages above 2.40 mm d^{-1} during all quarters. However, the highest ones were in *Q*1 (January to March), when the average surpassed 2.80 mm d^{-1}, while the lowest ones occurred from April to September (*Q*2 to *Q*3), below 2.50 mm d^{-1}. With an annual value of 953 mm yr^{-1}, Atlantic Forest showed the second highest ET rates, behind only the Pampa biome. From water balance studies in this biome, Pereira et al. (2010) found an average annual ET of 3.20 mm d^{-1}, a little higher than that from Table 2. However, also from water balance measurements taken between 2013 and 2018 in Atlantic Forest, Rodrigues et al. (2021) reported ET mean values from 1.40 to 1.80 mm d^{-1}, within the ranges for *Q*3 (July to September), represented by the mean pixel value and the SD of our study.

The highest ET rates for the Pampa biome happened in *Q*1 (January to March) and *Q*3 (July to September), when the mean pixel values were above 3.20 mm d^{-1}, while the lowest ones occurred in *Q*2 (April to June), when the average was below 2.60 mm d^{-1}. The high daily rates produced the highest annual ET of 1,098 mm yr^{-1} among biomes. From eddy covariance measurements taken between 2014 and 2016 in two distinct ecosystems of Pampa, Rubert et al. (2018) reported average ET values of 2.36 ± 1.40 and 2.56 ± 1.70 mm d^{-1}, involving our mean annual value, considering the ranges encompassed by the average and SD.

Considering all Brazilian biomes, the highest ET rates occurred from January to March ($Q1$), while the lowest ones happened from July to September ($Q3$). According to the SD values, the largest ET spatial variations occurred during $Q4$ (October to December) for Caatinga, when SD was 105% of the average, while the lowest ones happened in $Q1$ (January to March) for Pampa, when SD accounted for 22% of the average ET. Rainfall water variability is the main weather parameter driver for these variations, what may explain the large differences between the Northeast and Southeast regions where the Caatinga and Pampa biomes are located, respectively (see Figs. 1b and 4 and Table 1). The ET differences could be caused by distinct soil moisture levels, but they can also be controlled by the available energy (Seneviratne et al., 2010). However, it should be emphasized that other important reason for varying ET among biomes might be differences in soil covered by vegetation, which affect the absorbed solar radiation and partitions into transpiration and evaporation (Villalobos et al., 2013). The ET ranges from the current study are reasonably comparable with those in the literature, even considering our lower P values.

Accounting the P and ET rates by intercrossing Tables 1 and 2, the highest positive water balance ($P > \mathrm{ET}$) values occurred from January to March ($Q1$) for the Amazon ($\mathrm{WB} = 147$ mm) and Pantanal ($\mathrm{WB} = 1$ mm), but from October to December ($Q4$) in the Caatinga, Pampa, Atlantic Forest, and Cerrado biomes, with WB quarterly values of 84, 73, 53, and 52 mm Q^{-1}, respectively. The most negative water balance ($P < \mathrm{ET}$) happened from July to September ($Q3$) for the Pampa, Amazon, and Atlantic Forest biomes, with quarterly values of −70, −67, and −59 mm Q^{-1}, respectively; and, from April to June ($Q2$) for the Pantanal, Cerrado, and Caatinga, biomes, with quarterly values of −116, −96, and −86 mm Q^{-1}, respectively. On the annual scale, the most negative WB was detected for the Pantanal biome (average of −238 mm yr^{-1}), while the most positive WB occurred in the Amazon biome (average of 204 mm yr^{-1}). The first biome showed annual P of 578 mm yr^{-1} with a corresponding ET of 816 mm yr^{-1}, while for the Amazon these values were 1,009 mm yr^{-1} and 805 mm yr^{-1}. Although with similar ET rates, the greatest differences were on P values: those for Pantanal were half of those for Amazon.

Water productivity dynamics

Figure 5 shows the spatial distributions of the quarterly daily average biomass production (BIO), together with the mean pixel values and standard deviations (SD), for each Brazilian geographic region along the year 2016.

As for P and ET, spatial and temporal variations on BIO pixel values among quarters and geographic regions are also evident with the lowest values in the Northeast ($Q3$) where the Caatinga biome is concentrated and the highest ones in the South ($Q1$), with only the Pampa biome (see also Fig. 1). Intercrossing Figs. 1b and 5, Table 3 shows the quarterly and annually average values of biomass production (BIO) and standard deviations (SD) for each Brazilian biome during the year 2016, together with the pairwise comparisons by using Tuckey's honestly significant difference (HSD) post hoc test.

On the one hand, according to Tuckey's HSD test, there were statistical differences in BIO rates, mainly comparing the wettest biomes Atlantic Forest in $Q1$ (January to March) and Pampa during $Q1$ (January to March) and $Q3$ (July to September) with the driest Caatinga biome. On the other hand, there were no significant differences for Amazon from January to March ($Q1$), Cerrado from April to September ($Q2$ to $Q3$), and Pantanal from January to June ($Q1$ to $Q2$), when compared with Caatinga.

To infer the effect of root-zone conditions on the BIO rates (equation 13), Fig. 6 shows the quarterly average pixel values for the evapotranspiration fraction (ET_f), together with their standard deviations (SD) for each Brazilian biome.

The ET_f average values ranged between 0.14 in Caatinga from October to December ($Q4$) and 1.15 in Pampa from April to September ($Q3$). The respective annual averages were 0.29 and 0.94. In agreement with our results, de Teixeira et al. (2017) found ET_f values between 0.04 and 0.34 for the Caatinga biome using SAFER with Landsat 8 images, while Rubert et al. (2018) also reported small differences between ET and ET_0, with ET_f of 0.83 and 0.92 in two distinct Pampa ecosystems, throughout eddy covariance measurements taken from 2014 to 2016.

In pastures from Florida (USA), Sumner and Jacobs (2005) reported ET_f values ranging from 0.47 to 0.92 under irrigation conditions, while in steppes

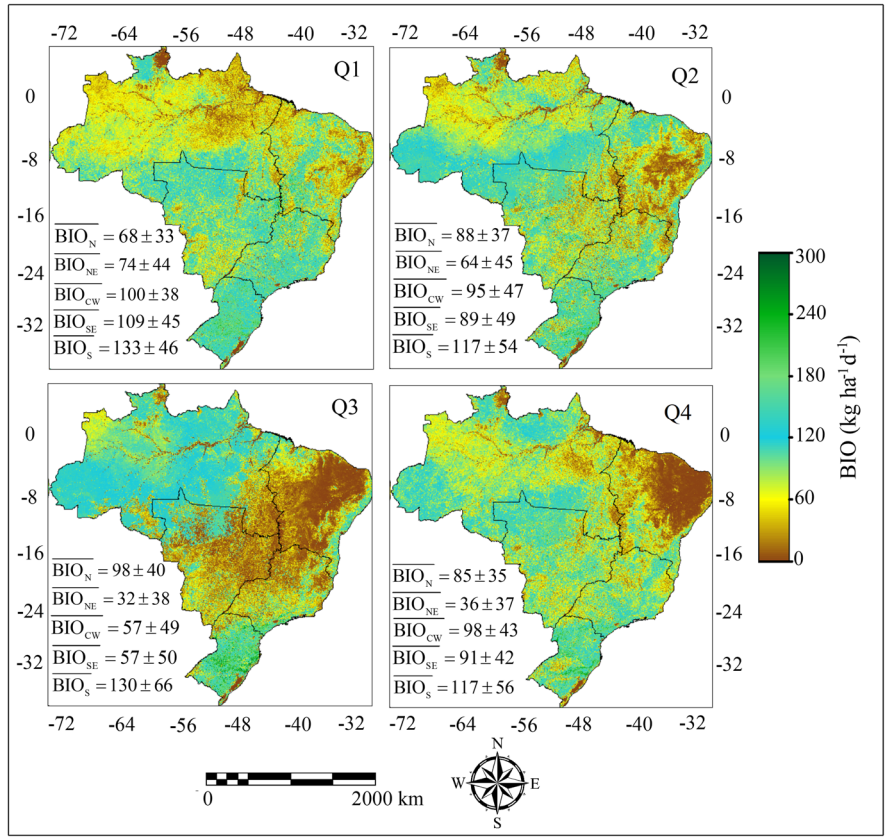

Fig. 5 Spatial distributions of the quarterly daily average biomass production (BIO) for each Brazilian geographic region, together with the mean pixel values and standard deviations (SD) during 2016. Overlines mean average BIO for the region. Quarters (*Q*): *Q*1—January to March, *Q*2—April to June, *Q*3—July to September, and *Q*4—October to December. Geographic regions: North—N, Northeast—NE, Central West—CW, Southeast—SE, and South—S

Table 3 Quarterly and annually average values of biomass production (BIO) and standard deviations (SD) for the Brazilian biomes during the year 2016, together with pairwise comparisons from Tuckey's honestly significant difference (HSD) post hoc test

Quarter[1]/biome[2]	*Q*1 (kg ha^{-1} d^{-1})	*Q*2 (kg ha^{-1} d^{-1})	*Q*3 (kg ha^{-1} d^{-1})	*Q*4 (kg ha^{-1} d^{-1})	Year (kg ha^{-1} d^{-1})
AM	72 ± 35a	93 ± 38b	101 ± 39b	89 ± 37b	89 ± 30b
CT	73 ± 42a	54 ± 43a	18 ± 28a	19 ± 28a	41 ± 25a
CE	96 ± 44b	78 ± 46a	37 ± 37a	79 ± 42b	72 ± 34b
PT	80 ± 38a	91 ± 37a	60 ± 36b	85 ± 42b	79 ± 35b
AF	114 ± 48c	104 ± 52b	95 ± 65b	104 ± 51b	104 ± 46b
PP	119 ± 52c	101 ± 57b	115 ± 67c	91 ± 55b	107 ± 50c
Mean	92 ± 43	87 ± 46	71 ± 45	78 ± 43	82 ± 37

[1]Quarters: *Q*1—January to March, *Q*2—April to June, *Q*3—July to September, and *Q*4—October to December. [2]Biomes: AM—Amazon, CT—Caatinga, CE—Cerrado, PT—Pantanal, AF—Atlantic Forest, and PP—Pampa. BIO values with the same letter in each column indicate no significant differences from each other at 5% (pairwise comparisons using Tuckey's HSD post hoc test for each quarter and for the whole year)

under desertic conditions of Mongolia, China, Zhang et al. (2012) found an ET_f range between 0.16 and 0.75. These values are similar in several situations depicted in Fig. 6, in which the lowest values were detected for the Caatinga and Cerrado biomes and the highest ones for the Pampa and Atlantic Forest biomes. According to Zhou and Zhou (2009), the climate variables that most affect ET_f are air temperature, air humidity, and available energy. However, its values will also depend on stomata aperture and adaptation of species to water scarcity (Mata-González et al., 2005), what is more visible in Caatinga and

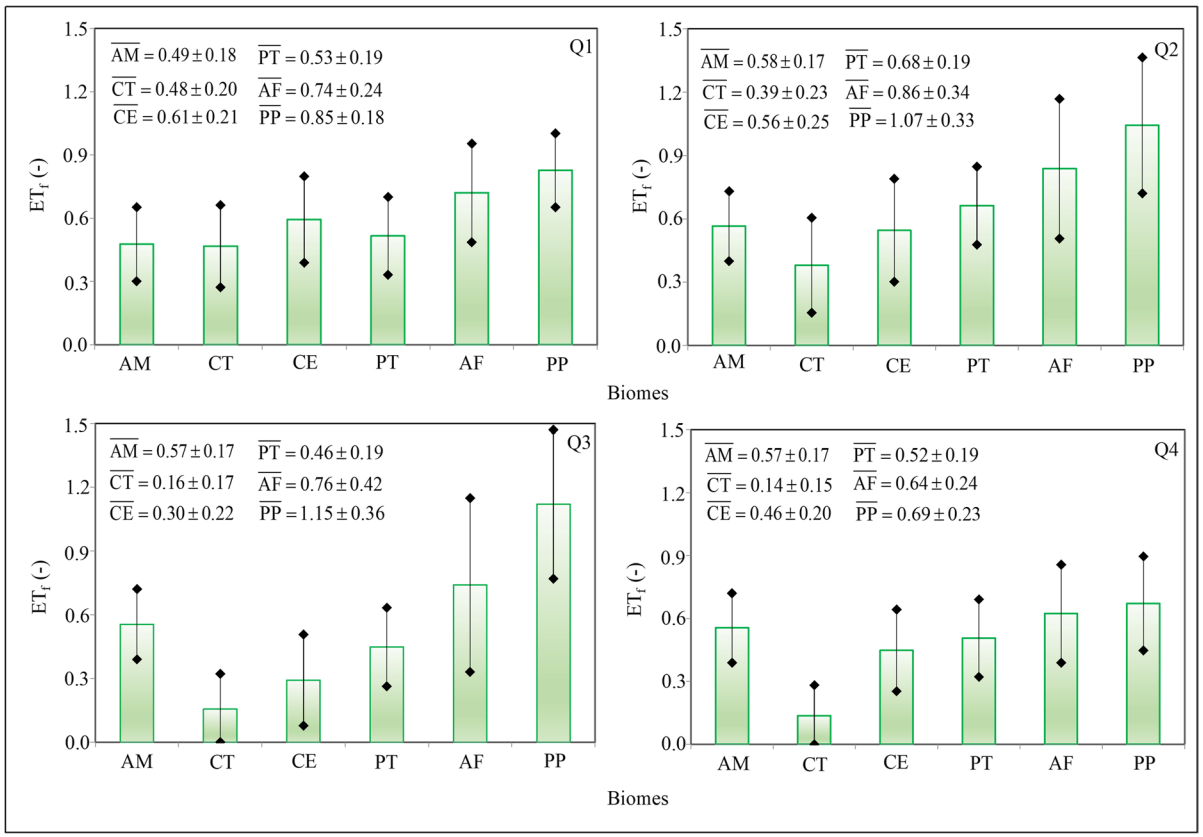

Fig. 6 Quarterly average pixel values for the evapotranspiration fraction (ET_f), together with the standard deviations (SD) during the year 2016. Overlines mean ET_f average pixel value for the biome. Quarters: *Q*1—January to March, *Q*2—April to June, *Q*3—July to September, and *Q*4—October to December. Biomes: Amazon—AM, Caatinga—CT, Cerrado—CE, Pantanal—PT, Atlantic Forest—AF, and Pampa—PP

Cerrado than in Pampa and Atlantic Forest biomes in Fig. 6.

Our results evidenced that there is a gap between ET_f and WB values along the year, which could be related to the time needed for recovering good soil moisture after rainfalls, but also because of some rainfall water is lost by runoff and percolation, what will affect BIO, and thus water productivity (WP) values.

Besides ET_f, BIO rates are also affected by absorbed photosynthetically active radiation (PAR_{abs}). Figure 7 presents the quarterly average PAR_{abs} values, together with standard deviations (SD) for each Brazilian biome.

From Table 3, for the Amazon biome, the maximum BIO occurred in *Q*3 (July to September), when the mean pixel value was above 100 kg ha^{-1} d^{-1}, because of a high ET_f (average of 0.57, Fig. 6) at its largest PAR_{abs} (around 6.86 MJ m^{-2} d^{-1}, Fig. 7). The minimum BIO values occurred in *Q*1 (January to March), when the average was below 75 kg ha^{-1} d^{-1}, under the lowest both ET_f (around 0.49, Fig. 6) and PAR_{abs} (mean of 5.71 MJ m^{-2} d^{-1}, Fig. 7). Regarding the annual scale, the average BIO for Amazon was 32.6 t ha^{-1} yr^{-1}. According to Vieira et al. (2003), BIO in this biome may vary across regions due to differences in edaphic, climatic, and historical land-use factors, thus rendering most relationships among spectral properties and site-specific forest age. In Central Amazon, from eddy covariance measurements taken between 2008 and 2011, in primary and secondary forests, von Randow et al. (2020) reported average BIO rates of 162 and 156 kg ha^{-1} d^{-1}, respectively. These values are higher than found in the current study.

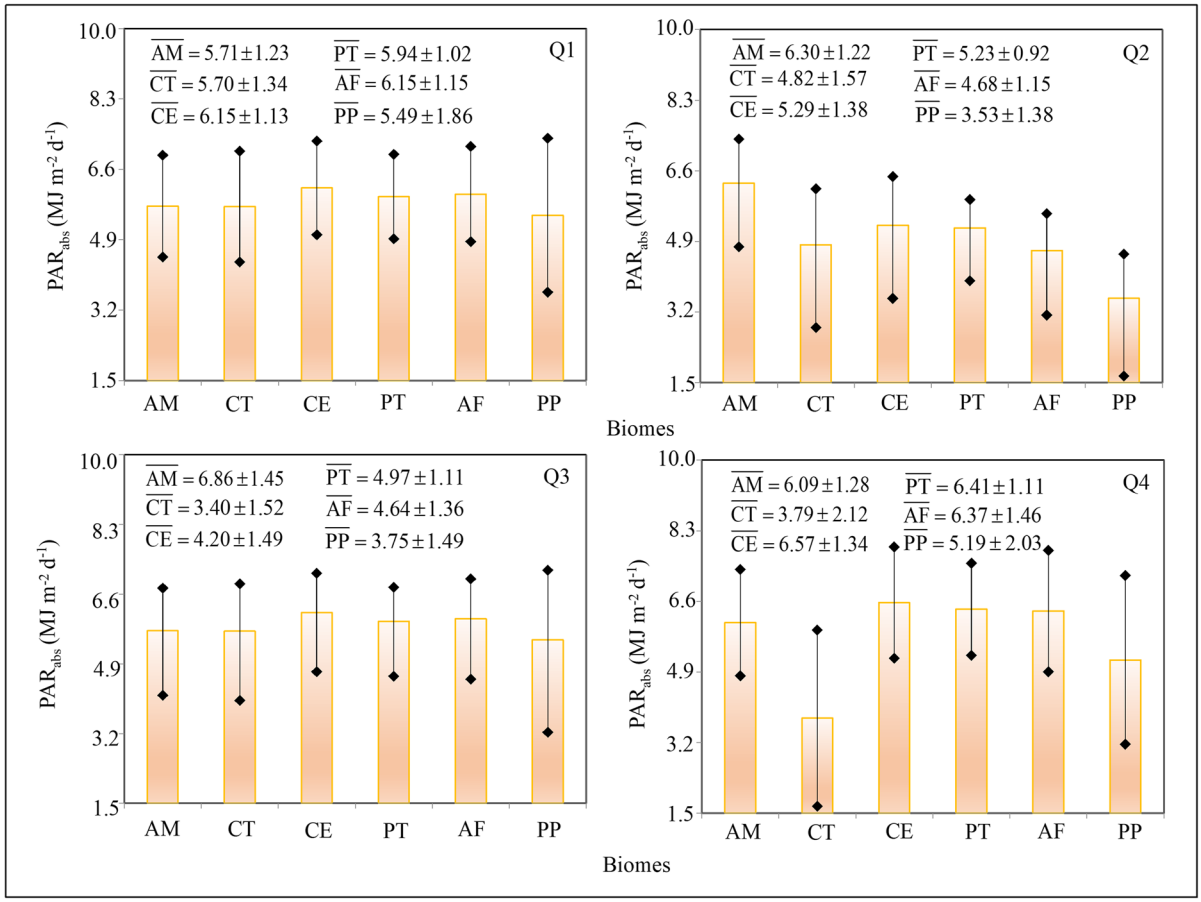

Fig. 7 Quarterly average values of the absorbed photosynthetically active radiation (PAR_{abs}), together with standard deviations (SD) for each Brazilian biome during the year 2016. Overlines mean PAR_{abs} average for the biome. Quarters: *Q*1—January to March, *Q*2—April to June, *Q*3—July to September, and Q4—October to December. Biomes: Amazon—AM, Caatinga—CT, Cerrado—CE, Pantanal—PT, Atlantic Forest—AF, and Pampa—PP

In Caatinga, the highest average BIO, above 70 kg ha^{-1} d^{-1}, happened during the rainiest quarter *Q*1 (January to March), when both the highest ET_f (average of 0.48, Fig. 6) and PAR_{abs} (around 5.70 MJ m^{-2} d^{-1}, Fig. 7) occurred. However, outside this period, from *Q*3 to *Q*4 (July to December), the mean BIO pixel value was below 20 kg ha^{-1} d^{-1} at both the lowest ET_f (average of 0.14 in *Q*4, Fig. 6) and PAR_{abs} (around 3.40 MJ m^{-2} d^{-1} in *Q*3, Fig. 7). The annual average was only 15.0 t ha^{-1} yr^{-1}, the lowest one among Brazilian biomes. From eddy flux measurements taken from 2014 to 2015 in Caatinga, da Silva et al. (2017) reported that its species act as atmospheric carbon sources during the driest periods yielding lower BIO, and as carbon sinks in the wettest periods promoting higher BIO. Pereira et al. (2020) confirm that BIO in the Caatinga biome decreases under water stress conditions, resulting in rapid changes in carbon dynamics, as these conditions affect phenology, seasonality of stomatal conductance, and photosynthesis. These previous works agree with the results in Table 3.

The highest BIO rates in Cerrado were detected in *Q*1 (January to March), when the average was above 95 kg ha^{-1} d^{-1}, at its highest mean ET_f of 0.61 (Fig. 6), together with a high PAR_{abs} (mean of 6.15 MJ m^{-2} d^{-1}, Fig. 7). The lowest BIO happened in *Q*3 (July to September), with a mean pixel value below 40 kg ha^{-1} d^{-1}, at both its lowest ET_f (average of 0.30, Fig. 6) and PAR_{abs} (mean pixel value of 4.20 MJ m^{-2} d^{-1}, Fig. 7). The mean annual BIO was 26.5 t ha^{-1} yr^{-1}, the second lowest value after the Caatinga biome. The seasonal behavior of BIO

in the Cerrado biome described in Table 3 is in accordance with Arantes et al. (2016), who, using the MODIS MOD13Q1 Enhanced Vegetation Index, reported that vegetation developments were maximum from January to March and decreased to half the values from August to September. BIO decline in *Q*3 (July to September) in the current study also agrees with dos Santos et al. (2021), who, using MODIS products, reported a reduction on BIO values in the Cerrado biome following rainfall declines (see also Table 1).

Although Pantanal showed the most negative annual water balance (WB) among biomes, its BIO rates were still higher than those for Caatinga and Cerrado. Maximum BIO, with mean pixel value above 90 kg ha^{-1} d^{-1}, occurred in *Q*2 (April to June), at the highest average ET_f of 0.68 (Fig. 6), together with a big mean PAR_{abs} of 5.23 MJ m^{-2} d^{-1} (Fig. 7). Minimum BIO rates, around 60 kg ha^{-1} d^{-1}, happened in *Q*3 (July to September), at its lowest both ET_f (average of 0.46, Fig. 6) and PAR_{abs} (around 4.97 MJ m^{-2} d^{-1}, Fig. 7). The annual BIO for Pantanal was 28.9 t ha^{-1} yr^{-1}. From Table 3, one may notice that differences in BIO values among quarters were not so large for this biome, what agrees with Pozer and Nogueira (2004), who reported no differences on BIO values for humid and dry months, because Pantanal terrestrial species may be replaced by its aquatic ones. However, according to Sanches et al. (2014), BIO in Pantanal is higher during the rainy season when solar radiation levels are large, what agrees with the period from January to June (*Q*1 to *Q*2) in the current study.

In the Atlantic Forest, BIO values were more constant along the year when compared with the previous biomes. The highest average, above 110 kg ha^{-1} d^{-1}, was detected in *Q*1 (January to March), at both high ET_f, mean of 0.74 (Fig. 6), and PAR_{abs}, average of 6.15 MJ m^{-2} d^{-1} (Fig. 7). The lowest BIO, around 95 kg ha^{-1} d^{-1}, happened in *Q*3 (July to September), at a mean ET_f of 0.76 (Fig. 6), under the lowest average PAR_{abs} of 4.64 MJ m^{-2} d^{-1} (Fig. 7). On the annual scale, the average BIO of 38.2 t ha^{-1} yr^{-1} was the second highest among biomes, behind only Pampa. Rebello et al. (2020), using MODIS images, reported that drought significantly impacted BIO in Atlantic Forest from 2012 to 2015, followed by a strong successive recovery pulse after the drier period. de Teixeira, Takemura, et al. (2020) applied the SAFER algorithm to MODIS images and found annual average BIO ranging from 47 to 93 kg ha^{-1} d^{-1} for this biome within the São Francisco River basin, corroborating our rates, considering the limits involved in the average and the SD values.

As for the Atlantic Forest, the Pampa biome also showed regular tendency on BIO values along the year; its maximum average was above 115 kg ha^{-1} d^{-1} in *Q*1 (January to March), at a high mean ET_f of 0.85 (Fig. 6) and the highest average PAR_{abs} of 5.49 MJ m^{-2} d^{-1} (Fig. 7). The minimum BIO rates occurred in *Q*4 (October to December), but the mean pixel value did not fall below 90 kg ha^{-1} d^{-1}, when the lowest mean ET_f of 0.69 (Fig. 6) occurred at an average PAR_{abs} of 5.19 MJ m^{-2} d^{-1} (Fig. 7). The Pampa biome showed the highest average annual BIO of 39.2 t ha^{-1} yr^{-1}, 2.6-folds that for Caatinga. Using remote sensing measurements taken from 2001 to 2011, Scottá and da Fonseca (2015) also found maximum BIO values during *Q*1 (January to March) for Pampa; however, they affirmed that BIO correlations with weather conditions should be considered for this biome. According to Rubert et al. (2018), plant diversity in Pampa is what determines the vegetation growth capacity during the seasons of the year, but it is also affected by the available energy, what agrees with our highest BIO values in *Q*1 (January to March), which showed the highest PAR_{abs} levels.

Considering all biomes, the quarterly periods with the highest BIO values occurred from July to September (*Q*3) for Amazon; from January to March (*Q*1) for Caatinga, Cerrado, Atlantic Forest, and Pampa; and from April to June (*Q*2) for Pantanal. The lowest BIO rates happened in *Q*1 (January to March) for Amazon; in *Q*3 (July to September) for Caatinga, Cerrado, Atlantic Forest, and Pantanal; and in *Q*4 (October to December) for Pampa. According to the SD values, the largest BIO spatial variations occurred during *Q*3 (July to September) for Caatinga, when SD was 156% of the average, while the lowest ones happened in *Q*3 (July to September) for Amazon, when SD accounted for 39% of the average.

For some biomes, BIO was more strongly related to ET_f (Cerrado, Caatinga, Pantanal, and Pampa biomes) while for others BIO rates followed the PAR_{abs} levels (Amazon and Atlantic Forest). As there is a correlation between ET and BIO, this can be explained by the fact that soil moisture provides a first-order control on BIO when water is limiting (i.e., low ET_f), while when ET_f is high (i.e., good soil moisture levels), BIO is more affected by the available energy (Seneviratne et al., 2010). One should

have highlight that in the current research, BIO is the daily biomass production and not the actual biomass, which is the reason why Atlantic Forest and Pampa showed higher BIO than Amazon, which has larger natural vegetated areas with trees. For example, a grassed surface may increase BIO faster from one day to another than taller surfaces.

Accounting for ET and BIO values by intercrossing Tables 2 and 3, the periods of the year with the highest water productivity (WP) values (equation 15) were from April to June (*Q*2) for the Atlantic Forest, Amazon, Pampa, and Pantanal, with respective WP of 4.32, 4.29, 3.93, and 3.91 kg m^{-3} and from January to March (*Q*1) for Cerrado and Caatinga, with respective WP of 3.61 and 3.08 kg m^{-3}. The lowest WP values occurred in *Q*1 (January to March) for Amazon, when it was 3.81 kg m^{-3}; *Q*3 (July to September) for Caatinga, Cerrado, Pantanal, and Atlantic Forest, with respective values of 2.25, 2.78, 3.09, and 3.82 kg m^{-3}; and from October to December (Q4) for Pampa, with WP of 3.06 kg m^{-3}. The strongest differences among biomes were detected for Amazon and Atlantic Forest, both with annual WP values of 4.00 kg m^{-3}, when compared with the driest Caatinga biome, with an annual WP of 2.80 kg m^{-3}.

To integrate vegetation growth and environmental conditions in the Brazilian biomes, Fig. 8 shows the relations among BIO, P, and ET, taking their quarterly average values during the year, for each Brazilian biome.

On one hand, there was negative correlation of BIO with *P* only for the Amazon and Pampa biomes (Fig. 8a), with the highest correlation for the first (R^2=0.77) than for the second (R^2=0.36). This means that some rainfall water was not productive, with more situations of water going away from the root zones and not being used by vegetation, mainly in the Amazon biome. On the other hand, this correlation was positive for Caatinga, Cerrado, Pantanal, and Atlantic Forest biomes, with the highest one for Caatinga (R^2=0.70) and the lowest one for Pantanal (R^2=0.13). Regarding the correlations of BIO with ET (Fig. 8b), they were positive for all biomes the with the highest ones for Caatinga and Cerrado (R^2=0.99), while the lowest correlation was for Pampa (R^2=41).

Caatinga biome stands up by the highest positive correlations in Fig. 8, what can be explained that this biome, under high solar radiation levels during the rainy periods, has a high-water consumption yielding large BIO. In Pampa biome, even with large rainfall amounts promoting large ET_f values (Fig. 6), the gap in water balance and soil moisture conditions together with low PAR_{abs} levels (Fig. 7) promoted the lowest correlation of BIO to ET.

Conclusions

We demonstrated the suitability of the SAFER algorithm for use with MODIS' MOD13Q1 reflectance product and gridded weather data to monitor the dynamics of environmental remote sensing indicators in the Brazilian biomes, derived from energy, water, and carbon balance components. According to Tukey's honestly significant difference (HSD) post hoc test, significant differences in precipitation (*P*), actual evapotranspiration (ET), and biomass production (BIO) yielded distinct water balance (WB) and water productivity (WP) results. The largest WB and WP differences among biomes were detected for the Atlantic Forest and Pampa, when compared with the driest Caatinga biome.

Rainfall variability is the main responsible weather parameter driver for the spatial ET and BIO variations, which explains the large differences between Caatinga and Pampa. It should be emphasized that varying ET might also be caused by different areas of soil covered by the vegetation within these biomes, affecting the partitions into transpiration and evaporation. Amazon showed the highest positive WB among biomes, while Pantanal showed the most negative WB, evidencing that agroecosystems in this last biome were strongly affected by water scarcity during 2016.

Rainfall distribution along the year in each biome also contributed to the magnitude of the evaporative fraction (ET_f). However, there were gaps between ET_f and WB, which may be related to the time needed for recovering good conditions of soil moisture levels after rainfalls, but also because some of the rainfall water is lost by runoff and percolation, what also affects BIO, and thus WP. On one hand, these rainfall water lost produced negative correlations between BIO and *P* in the Amazon and Pampa biome. On the other hand, the most positive relations for both BIO with *P* and with ET were for Caatinga, because of the fast response of their species to rainfalls. The highest WP was detected for the Amazon biome, while the lowest WP happened in Caatinga. For the Amazon and Atlantic Forest biomes, BIO rates were much related to the levels of absorbed photosynthetically

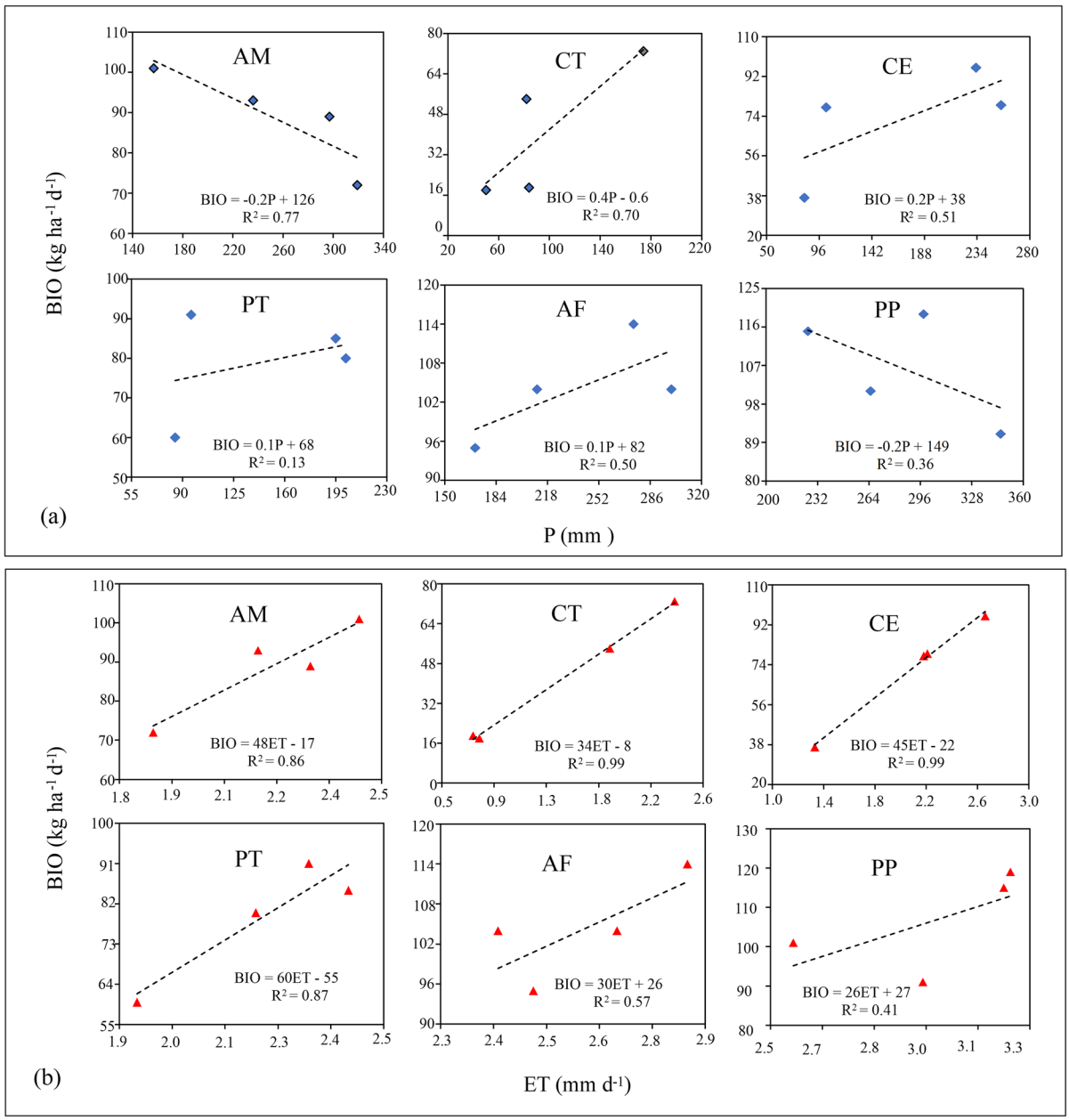

Fig. 8 Relations between the quarterly values for biomass production (BIO) with those for precipitation (*P*) and actual evapotranspiration (ET) in each Brazilian biome during the year 2016. Biomes: Amazon—AM, Caatinga—CT, Cerrado—CE, Pantanal—PT, Atlantic Forest—AF, and Pampa—PP

active radiation, while for the Cerrado, Caatinga, Pantanal, and Pampa biomes, ET_f values affected more BIO values.

Although the methods were tested for only one year in the current research, the success of the coupled use of MODIS' MOD13Q1 reflectance product and gridded weather data showed potential for the implementation of an operational environmental monitoring system by using historical data sets, with enough details to differentiate the Brazilian biomes using remote-sensing indicators. The spatial determinations of ET and BIO and their association with precipitation

gridded data showed with good potential to support public policies regarding the management and conservation of natural resources, with possibility for replication of the methods in other countries, after local calibrations of the regression equations. Limitations for application of the methods in other environments could be lack of meteorological data on large scales and the probable need of equation calibrations which will demand simultaneous field and satellite measurements. Future research may focus on detecting water balance and water productivity anomalies for specific years in comparison with long-term conditions.

Acknowledgements To National Meteorological Institute (INMET) for weather data availability.

Author contribution Antônio Teixeira was responsible for running the models, conceptualizations, energy, water, and carbon balance assessments and writing the manuscript, designing of figures, result analyses, software resources, and supervision. Janice Leivas oversaw running of scripts, download and processing MODIS images MODIS images, and formatting of the weather data, methodology, data curation, and editing of the manuscript. Celina Takemura helped on downloading and processing MODIS images, weather data processing, and result analyses. Gustavo Bayma acted on downloading/processing MODIS images and weather data. Edlene Garçon acted on downloading/processing MODIS images and weather data. Inajá Sousa acted on downloading/processing MODIS images and weather data. Franzone Farias acted on processing MODIS images and weather data. Cesar Silva helped with statistical analyzes.

Data availability Raw weather data were from the Brazilian National Meteorological Institution (INMET - https://www.gov.br/agricultura/pt-br/assuntos/inmet), shape files used are available by the Statistical and Geographic Brazilian Institute (IBGE - www.ibge.gov.br), and the MODIS products were downloaded from the EARTHDATA AppEEARS's site (https://lpdaacsvc.cr.usgs.gov/appeears/). Derived data supporting the findings of this study are available from the corresponding author on request.

Declarations

Competing interests The authors declare no competing interests.

References

Allen, R. G., Pereira, L. S., Raes, D., & Smith, M. (1998). *Crop evapotranspiration, Guidelines for computing crop water requirements*. FAO Irrigation and Drainage Paper 56.

Almagro, A., Oliveira, P. T. S., & Nearing, M. A. (2017). Projected climate change impacts in rainfall erosivity over Brazil. *Scientific Reports, 7*, 8130.

Arantes, A. E., Ferreira, L. G., & Coe, M. T. (2016). The seasonal carbon and water balances of the Cerrado environment of Brazil: Past, present, and future influences of land cover and land use. *ISPRS Journal Photogrammetry and Remote Sensing, 117*, 66–78.

Araujo, L. M., de Teixeira, A. H. C., & Bassoi, L. H. (2019). Evapotranspiration and biomass modelling in the Pontal Sul Irrigation Scheme. *International Journal of Remote Sensing, 41*, 2326–2338.

Assine, M. L., Merino, E. R., do Nascimento Pupim, F., de Azevedo Macedo, H., & dos Santos, M. G. M. (2015). The Quaternary alluvial systems tract of the Pantanal basin, Brazil. *Brazilian Journal of Geology, 45*, 475–489.

Bastiaanssen, W. G. M., & Ali, S. (2003). A new crop yield forecasting model based on satellite measurements applied across the Indus Basin, Pakistan. *Agriculture, Ecosystems & Environment, 94*, 321–340.

Bhattarai, N., Wagle, P., Gowda, P. H., & Kakani, V. G. (2017). Utility of remote sensing-based surface energy balance models to track water stress in rain-fed switchgrass under dry and wet conditions. *ISPRS Journal Photogrammetry and Remote Sensing, 113*, 128–141.

Cabral, O. M. R., Rocha, H. R., Gash, J. H., Freitas, H. C., & Ligo, M. A. V. (2015). Water and energy fluxes from a woodland savanna (Cerrado) in southeast Brazil. *Journal of Hydrology, 4*, 22–40.

Casagrande, E., Recanati, F., Rulli, M. C., Bevacqua, D., & Meli, P. (2021). Water balance partitioning for ecosystem service assessment. A case study in the Amazon. *Ecological Indicators, 121*, 107155.

Ceschia, E., Beziat, P., Dejoux, J. F., Aubinet, M., Bernhofer, C., Bodson, B., Buchmann, N., Carrara, A., Cellier, P., Di Tommasi, P., Elbers, J. A., Eugster, W., Grünwald, T., Jacobs, C. M. J., Jans, W. W. P., Jones, M., Kutsch, W., Lanigan, G., Magliulo, E., et al. (2010). Management effects on net ecosystem carbon and GHG budgets at European crop sites. *Agriculture, Ecosystems & Environment, 139*, 363–383.

Claverie, M., Demarez, V., Duchemin, B., Hagolle, O., Ducrot, D., Marais-Sicre, C., Dejoux, J.-F., Huc, M., Keravec, P., Béziat, P., Fieuzal, R., Ceschia, E., & Dedieu, G. (2012). Maize and sunflower biomass estimation in southwest France using spatial and temporal resolution remote sensing data. *Remote Sensing of Environment, 124*, 884–857.

Cleugh, H. A., Leuning, R., Mu, Q., & Running, S. W. (2007). Regional evaporation estimates from flux tower and MODIS satellite data. *Remote Sensing of Environment, 106*, 285–304.

Consoli, S., Licciardello, F., Vanella, D., Pasotti, L., Villani, G., & Tomei, F. (2016). Testing the water balance model CRITERIA using TDR measurements, micrometeorological data, and satellite-based information. *Agricultural Water Management, 170*, 68–80.

Consoli, S., & Vanella, D. (2014). Comparisons of satellite-based models for estimating evapotranspiration fluxes. *Journal of Hydrology, 513*, 475–489.

da Silva, P. F., de Lima, J. R. S., Antonino, A. C. D., Souza, R., de Souza, E. S., Silva, J. R. I., & Alves, E. M. (2017). Seasonal patterns of carbon dioxide, water, and energy fluxes over the Caatinga and grassland in the semi-arid region of Brazil. *Journal of Arid Environments, 147*, 71–82.

de Almeida, S. L. H., Souza, J. B. C., Nogueira, S. F., Pezzopane, J. R. M., de Teixeira, A. H. C., Bosi, C., Adami, M., Zerbato, C., Bernardi, A. C. C., Bayma, G., & da Silva, R. P. (2023). Forage mass estimation in silvopastoral and full sun systems: Evaluation through proximal remote sensing applied to the SAFER model. *Remote Sensing, 15*, 815.

de Almeida, S. L. H., Souza, J. B. C., Pilon, C., de Teixeira, A. H. C., do Santos, A. F., Sysskind, M. N., Vellidis, G., & da Silva, R. P. (2023). Performance of the SAFER model in estimating peanut maturation. *European Journal of Agronomy, 147*, 126844–126810.

de Azevedo, G. B., Rezende, A. V., Azevedo, G. T. O. S., Miguel, E. P., Aquino, F. G., Bruzinga, J. S. C., de Oliveira, L. S. C., Pereira, R. S., & Teodoro, P. E. (2020). Woody biomass accumulation in a Cerrado of Central Brazil monitored for 27 years after the implementation of silvicultural systems. *Forest Ecology and Management, 455*, 117718.

de Bruin, H. A. R. (1987). From Penman to Makkink. In J. C. Hooghart (Ed.), *Proceedings and information: TNO committee on hydrological sciences* (Vol. 39, pp. 5–31). Gravenhage.

de Silva, A. L. C., & De Costa, W. A. J. M. (2012). Growth and radiation use efficiency of sugarcane under irrigated and rain-fed conditions in Sri Lanka. *Sugar Tech, 14*, 247–254.

de Teixeira, A. H. C. (2010). Determining regional actual evapotranspiration of irrigated and natural vegetation in the São Francisco River basin (Brazil) using remote sensing and Penman-Monteith equation. *Remote Sensing, 2*, 1287–1319.

de Teixeira, A. H. C., Bastiaanssen, W. G. M., Ahmad, M. D., Moura, M. S. B., & Bos, M. G. (2008). Analysis of energy fluxes and vegetation-atmosphere parameters in irrigated and natural ecosystems of semi-arid Brazil. *Journal of Hydrology, 362*, 110–127.

de Teixeira, A. H. C., Leivas, J. F., Garçon, E. A. M., Takeura, C. M., Quartaroli, C. F., & Alvarez, I. A. (2020). Modeling large-scale biometeorological indices to monitor agricultural-growing areas: Applications in the fruit circuit region, São Paulo, Brazil. *International Journal of Biometeorology, 1*, 1–14.

de Teixeira, A. H. C., Leivas, J. F., Pacheco, E. P., Garçon, E. A. M., & Takemura, C. M. (2021). Biophysical characterization and monitoring large-scale water and vegetation anomalies by remote sensing in the agricultural growing areas of the Brazilian semi-arid region. In P. C. Pandey & L. K. Sharma (Eds.), *Advances in remote sensing for natural resource monitoring* (1st ed., pp. 94–109). Wiley Online Library.

de Teixeira, A. H. C., Leivas, J. F., & Silva, G. B. (2017). Drought assessments by coupling Moderate Resolution Imaging Spetroradiometer images and weather data: A case study in the Minas Gerais state, Brazil. In G. P. Petropoulos & T. Islam (Eds.), *Remote sensing of hydrometeorological hazards* (1st ed., pp. 53–68). CRR Press.

de Teixeira, A. H. C., Leivas, J. F., Struiving, T. B., Reis, J. B. R. S., & Simão, F. R. (2021). Energy balance and irrigation performance assessments in lemon orchards by applying the SAFER algorithm to Landsat 8 images. *Agricultural Water Management, 247*, 1–9.

de Teixeira, A. H. C., Scherer-Warren, M., Hernandez, F. B. T., Andrade, R. G., & Leivas, J. F. (2013). Large-scale water productivity assessments with MODIS Images in a changing semi-arid environment: A Brazilian case study. *Remote Sensing, 5*, 5783–5804.

de Teixeira, A. H. C., Simão, F. R., Leivas, J. F., Gomide, R. L., Reis, J. B. R. S., Kobayashi, M. K., & Oliveira, F. G. (2018). Water productivity modeling by remote sensing in the semiarid region of Minas Gerais state, Brazil. In I. Yuksel & H. Arman (Eds.), *Arid environments and sustainability* (1st ed., pp. 94–108). InTech.

de Teixeira, A. H. C., Takemura, C. M., Leivas, J. F., Pacheco, E. P., Silva, G. B., & Garçon, E. A. M. (2020). Water productivity monitoring by using geotechnological tools in contrasting social and environmental conditions: Applications in the São Francisco River basin, Brazil. *Remote Sensing Applications: Society and Environment, 18*, 1–9.

Dehziari, S. A., & Sanaienejad, S. H. (2019). Energy balance quantification using Landsat 8 images and SAFER algorithm in Mashhad, Razavi Khorasan, Iran. *Journal of Applied Remote Sensing, 13*, 014528.

dos Santos, G. L., Pereira, M. G., Delgado, R. C., Magistrali, I. C., da Silva, C. G., de Oliveira, C. M. M., Laranjeira, J. P. B., & da Silva, T. P. (2021). Degradation of the Brazilian Cerrado: Interactions with human disturbance and environmental variables. *Forest Ecology and Management, 482*, 118875.

Fernandes, F. H. S., Sano, E. E., Ferreira, L. G., de Mello Baptista, G. M., de Castro Victoria, D., & Fassoni-Andrade, A. C. (2018). Degradation trends on MODIS derived estimates of productivity and water use efficiency: A case study for the cultivated pastures in the Brazilian Cerrado. *Remote Sensing Applications: Society and Environment, 11*, 30–40.

Franco, R. A., Hernandez, F. B., Teixeira, A. H. D. C., Leivas, J. F., Coaguila, D. N., & Neale, C. M. (2016). Water productivity mapping using Landsat 8 satellite together with weather stations. *Proceedings of SPIE, 9998*, 99981H-1–99981H-12.

Giambelluca, T. W., Scholz, F. G., Bucci, S. J., Meinzer, F. C., Goldstein, G., Hoffmann, W. A., Franco, A. C., & Bucherta, M. P. (2009). Evapotranspiration and energy balance of Brazilian savannas with contrasting tree density. *Agricultural and Forest Meteorology, 149*, 1365–1376.

Jardim, A. M. D. R. F., Araújo Júnior, G. D. N., Silva, M. V. D., Santos, A. D., Silva, J. L. B. D., Pandorfi, H., Oliveira-Júnior, J. F. D., Teixeira, A. H. D. C., Teodoro, P. E., de Lima, J. L., & Silva Junior, C. A. D. (2022). Using remote sensing to quantify the joint effects of climate and land use/land cover changes on the Caatinga biome of Northeast Brazilian. *Remote Sensing, 14*, 1911.

Kunert, N., Aparecido, L. M. T., Wolff, S., Higuchi, N., Santos, J., Araujo, A. C., & Trumbore, S. (2017). A revised hydrological model for the Central Amazon: The importance of emergent canopy trees in the forest water budget. *Agricultural and Forest Meteorology, 239*, 47–57.

Laipelt, L., Ruhoff, A. L., Fleischmann, A. S., Kayser, R. H. B., de Kich, E. M., da Rocha, H. R., & Neale, C. M. U. (2020). Assessment of an automated calibration of the SEBAL algorithm to estimate dry-season surface-energy partitioning in a Forest–Savanna transition in Brazil. *Remote Sensing, 12*, 1108.

Lathuillière, M. J., Dalmagro, H. J., Black, T. A., de Arruda, P. H. Z., Hawthorne, I., Couto, E. G., & Johnson, M. S. (2018). Rain-fed and irrigated cropland-atmosphere water fluxes, and their implications for agricultural production in Southern Amazonia. *Agricultural and Forest Meteorology, 256-257*, 407–419.

Leivas, J. F., de Teixeira, A. H. C., Andrade, R. G., de Victoria, D. C., Silva, G. B., & Bolfe, E. L. (2015). Application of agrometeorological spectral model in rice area in southern Brazil. *Proceedings of SPIE, 9637*, 96372B-1–96372B-8.

Lewinsohn, T. M., & Prado, P. I. (2005). How many species are there in Brazil? *Conservation Biology, 19*, 619–624.

Marengo, J. A., Cunha, A. P., Cuartas, L. A., Leal, K. R. D., Broedel, E., Seluchi, M. E., Michelin, C. M., Baião, C. F. P., Ângulo, E. C., Almeida, E. K., Kazmierczak, M. L., Mateus, N. P. A., Silva, R. C., & Bender, F. (2021). Extreme drought in the Brazilian Pantanal in 2019–2020: Characterization, causes, and impacts. *Frontiers in Water, 3*, 639204.

Mariano, D. A., dos Santos, C. A. C., Wardlowa, B. D., Anderson, M. C., Schiltmeyera, A. V., Tadessea, T., & Svoboda, M. D. (2018). Use of remote sensing indicators to assess effects of drought and human induced land degradation on ecosystem health in Northeastern Brazil. *Remote Sensing of Environment, 213*, 129–143.

Marin, F. R., Angelocci, L. R., Nassif, D. S. P., Vianna, M. S., Pilau, F. G., da Silva, E. H. M., Sobenko, L. R., Gonçalves, A. O., Pereira, R. A. A., & Carvalho, K. S. (2019). Revisiting the crop coefficient–reference evapotranspiration procedure for improving irrigation management. *Theoretical and Applied Climatology, 138*, 1785–1793.

Marques, T. V., Mendes, K., Mutti, P., Medeiros, S., Silva, L., Perez-Marin, A. M., Campos, S., Lúcio, P. S., Lima, K., dos Reis, J., Ramos, T. M., da Silva, D. F., Oliveira, C. P., Costa, G. B., Antonino, A. C. D., Menezes, R. S. C., Santos e Silva, C. M., & Bergson, B. B. (2020). Environmental and biophysical controls of evapotranspiration from seasonally dry tropical forests (Caatinga) in the Brazilian semiarid. *Agricultural and Forest Meteorology, 287*, 107957.

Mata-González, R., Mclendon, T., & Matin, D. W. (2005). The inappropriate use of crop transpiration coefficients (K_c) to estimate evapotranspiration in arid ecosystems: A review. *Arid Land Research and Management, 19*, 285–295.

Mateos, L., González-Dugo, M. P., Testi, L., & Villalobos, F. J. (2013). Monitoring evapotranspiration of irrigated crops using crop coefficients derived from time series of satellite images. I. Method validation. *Agricultural Water Management, 125*, 81–91.

Molden, D., Oweis, T., Steduto, P., Kijne, J. W., Hanjra, M. A., & Bindraban, P. S. (2007). Pathways for increasing agricultural water productivity. In R. Ross-Larson & C. Trott (Eds.), *Water for food, water for life: A comprehensive assessment of water management in agriculture* (pp. 279–310). International Water Management Institute.

Monteith, J. L. (1972). Solar radiation and productivity in tropical ecosystems. *Journal of Applied Ecology, 9*, 747–766.

Monteith, J. L. (1977). Climate and efficiency of crop production in Britain. *Philosophical Transactions of the Royal Society B, 281*, 277–294.

Moreira, A. A., Fassoni-Andrade, A. C., Ruhoff, A. L., & de Paiva, R. C. D. (2019). Water balance based on remote sensing data in Pantanal. *Raega-O Espaço Geográfico em Análise, 46*, 20–32.

Nagler, P. L., Glenn, E. P., Nguyen, U., Scott, R. L., & Doody, T. (2013). Estimating riparian and agricultural actual evapotranspiration by reference evapotranspiration and MODIS enhanced vegetation index. *Remote Sensing, 5*, 3849–3871.

Nobre, C. A., Sampaio, G., Borma, L. S., Castilla-Rubio, J. C., Silva, J. S., & Cardoso, M. (2016). The fate of the Amazon Forests: Land-use and climate change risks and the need of a novel sustainable development paradigm. *Proceedings of the National Academy of Sciences of the United States, 113*, 10759–10768.

Nuñez, D. C., Hernandez, F. B. T., de Teixeira, A. H. C., Franco, R. A. M., & Leivas, J. F. L. (2017). Water productivity using SAFER - Simple Algorithm for Evapotranspiration Retrieving in watershed. *Revista Brasileira de Engenharia Agrícola e Ambiental, 21*, 524–529.

Nyolei, D., Nsaali, M., Minaya, V., van Griensven, A., Mbilinyi, B., Diels, J., Hessels, T., & Kahimba, F. (2019). High resolution mapping of agricultural water productivity using SEBAL in a cultivated African catchment, Tanzania. *Physics and Chemistry of the Earth, 112*, 36–39.

Olivera-Guerra, L., Merlin, O., Er-Raki, S., Khabba, S., & Escorihuela, M. J. (2018). Estimating the water budget components of irrigated crops: combining the FAO-56 dual crop coefficient with surface temperature and vegetation index data. *Agricultural Water Management, 208*, 120–131.

Pereira, D. R., de Mello, C. R., da Silva, A. M., & Yanagi, S. N. M. (2010). Evapotranspiration and estimation of aerodynamic and stomatal conductance in a fragment of Atlantic Forest in Mantiqueira range region, MG. *Cerne, 16*, 32–40.

Pereira, M. P. S., Mendes, K. R., Justino, F. J., Couto, F., da Silva, A. S., da Silva, D. F., & Malhado, A. C. M. (2020). Brazilian dry forest (Caatinga) response to multiple ENSO: The role of Atlantic and Pacific Ocean. *Science of the Total Environment, 705*, 135717.

Pozer, C. G., & Nogueira, F. (2004). Flooded native pastures of the Northern region of the Pantanal of Mato Grosso: Biomass and primary productivity variations. *Brazilian Journal of Biology, 64*, 859–866.

Rampazo, N. A. M., Picoli, M. C. A., de Teixeira, A. H. C., & Cavaleiro, C. K. N. (2020). Water consumption modeling by coupling MODIS images and agrometeorological data for sugarcane crops. *Sugar Tech, 23*, 524–535.

Raupasch, M. R. (2001). Combination theory and equilibrium evaporation. *Quarterly Journal of Royal Meteorology Society, 127*, 1149–1181.

Rebello, V. P. A., Getirana, A., Filho, O. C. R., & Lakshmi, V. (2020). Spatiotemporal vegetation response to extreme droughts in eastern Brazil. *Remote Sensing Applications: Society and Environment, 18*, 100294.

Ribeiro, M. C., Metzger, J. P., Martensen, A. C., Ponzoni, F. J., & Hirota, M. M. (2009). The Brazilian Atlantic Forest: How much is left, and how is the remaining forest distributed? Implications for conservation. *Biological Conservation, 142*, 1141–1153.

Rodrigues, A. F., de Mello, C. R., Terra, M. C. N. S., & Beskow, S. (2021). Water balance of an Atlantic Forest remnant under a prolonged drought period. *Ciência e Agrotecnologia, 45*, e008421.

Roesch, L. F. W., Vieira, F. C. B., Pereira, V. A., Schünemann, A. L., Teixeira, I. F., Senna, A. J. T., & Stefenon, V. M. (2009). The Brazilian Pampa: A fragile biome. *Diversity, 1*, 182–198.

Rubert, G. C., Roberti, D. R., Pereira, L. S., Quadros, F. L. F., de Velho, H. F. C., & de Moraes, O. L. L. (2018). Evapotranspiration of the Brazilian Pampa biome: Seasonality and influential factors. *Water, 10,* 1864. https://doi.org/10.3390/w10121864

Safre, A. L. S., Nassar, A., Torres-Rua, A., Aboutalebi, M., Saad, J. C. C., Manzione, R. L., de Teixeira, A. H. C., Prueger, J. H., McKee, L. G., Alfieri, J. G., Hipps, L. E., Nieto, H., White, W. A., del Alsina, M. M., Sanchez, L., Kustas, W. P., Dokoozlian, N., Gao, F., & Anderson, M. C. (2022). Performance of Sentinel-2 SAFER ET model for daily and seasonal estimation of grapevine water consumption. *Irrigation Science, 40*, 635–654.

Sanches, L., da Silva, L. B., de Lima, S. D., Pereira, O. A., Carrilho, S. F. J., & Nogueira, J. S. (2014). Estoque de energia na biomassa e no ar do dossel de Vochysia divergens. Pohl. *Revista Brasileira de Engenharia Agrícola e Ambiental, 18*, 955–962.

Sanches, L., Vourlitis, G. L., Alves, M. C., Pinto-Júnior, O. B., & Nogueira, J. S. (2011). Seasonal patterns of evapotranspiration for a Vochysia divergens forest in the Brazilian Pantanal. *Wetlands, 31*, 1215–1225.

Sano, E. E., Rodrigues, A. A., Martins, E. S., Bettiol, G. M., Bustamante, M. M. C., Bezerra, A. S., Couto, A. F., Vasconcelos, V., Schüler, J., & Bolfe, E. L. (2019). Cerrado ecoregions: A spatial framework to assess and prioritize Brazilian savanna environmental diversity for conservation. *Journal of Environmental Management, 232*, 818–828.

Santos, J. E. O., Cunha, F. F., Filgueiras, R., Silva, G. H., de Teixeira, A. H. C., Silva, F. C. S., & Sediyama, G. C. (2020). Performance of SAFER evapotranspiration using missing meteorological data. *Agricultural Water Management, 233*, 1–8.

Santos, M. G., Oliveira, M. T., & Figueiredo, K. V. (2014). Caatinga, the Brazilian dry tropical forest: Can it tolerate climate changes? *Theoretical and Experimental Plant Physiology, 26*, 83–99.

Scottá, F. C., & da Fonseca, E. L. (2015). Multiscale trend analysis for Pampa grasslands using ground data and vegetation sensor imagery. *Sensors, 15*, 17666–17692.

Seneviratne, S. I., Corti, T., Davin, E. L., Hirschi, M., Jaeger, E. B., Lehner, I., Orlowsky, B., & Teuling, A. J. (2010). Investigating soil moisture–climate interactions in a changing climate: A review. *Earth-Science Reviews, 99*, 125–161.

Silva, C. O. F., de Teixeira, A. H. C., & Manzione, R. L. (2019). An R package for spatial modelling of energy balance and actual evapotranspiration using satellite images and agrometeorological data. *Environmental Modelling & Software, 120*, 104497.

Souza, C. M. Z., Jr., Shimbo, J., Rosa, M. R., Parente, L. L., Alencar, A., Rudorff, B. F. T., Hasenack, H., Matsumoto, M. G., Ferreira, L., Souza-Filho, P. W. M., de Oliveira, S. W., Rocha, W. F., Fonseca, A. V., Marques, C. B., Diniz, C. G., Costa, D., Monteiro, D., Rosa, E. R., Vélez-Martin, E., et al. (2020). Reconstructing three decades of land use and land cover changes in Brazilian biomes with Landsat archive and Earth Engine. *Remote Sensing, 12*, 2735.

Sumner, D. M., & Jacobs, J. (2005). Utility of penman-Monteith, Priestley-Taylor, reference evapotranspiration, and pan evaporation methods to estimate pasture evapotranspiration. *Journal of Hydrology, 308*, 81–104.

van Heerden, P. D. R., Donaldson, R. A., Watt, D. A., & Singels, A. (2010). Biomass accumulation in sugarcane: Unravelling the factors underpinning reduced growth phenomena. *Journal of Experimental Botany, 61*, 2877–2887.

Vanella, D., Ramírez-Cuesta, J. M., Intrigliolo, D. S., & Consoli, S. (2019). Combining electrical resistivity tomography and satellite images for improving evapotranspiration estimates of citrus orchards. *Remote Sensing, 11*, 373.

Venancio, L. P., Mantovani, E. C., do Amaral, C. H., Neale, C. M. U., Filgueiras, R., Gonçalves, I. Z., & da Cunha, F. F. (2021). Evapotranspiration mapping of commercial corn fields in Brazil using SAFER algorithm. *Scientia Agricola, 78*, 1–12.

Vieira, I. C. G., de Almeida, A. S., Davidson, E. A., Stone, T. A., de Carvalho, C. J. R., & Guerreiro, J. B. (2003). Classifying successional forests using Landsat spectral properties and ecological characteristics in eastern Amazônia. *Remote Sensing of Environment, 87*, 470–481.

Villalobos, F. J., Testi, L., Orgaz, F., García-Tejera, O., Lopez-Bernal, A., González-Dugo, M. V., Ballester-Lurbe, C., Castel, J. R., Alarcón-Cabañero, J. J., & Nicolás-Nicolás, E. (2013). Modelling canopy conductance and transpiration of fruit trees in Mediterranean areas: A simplified approach. *Agricultural and Forest Meteorology, 171*, 93–103.

von Randow, R. C. S., Tomasellac, J., von Randow, C., Araújo, A. C., Manzie, A. O., Hutjesf, R., & Kruijt, B. (2020). Evapotranspiration and gross primary productivity of secondary vegetation in Amazonia inferred by eddy covariance. *Agricultural and Forest Meteorology, 294*, 108141.

Yang, Y., Guan, H., Batelaan, O., McVicar, T. R., Long, D., Piao, S., Liang, W., Liu, B., Jin, Z., & Simmons, C. T. (2016). Contrasting responses of water use efficiency to drought across global terrestrial ecosystems. *Scientific Reports, 6*, 1–8.

Zhang, F., Zhou, G., Wang, Y., Yan, F., & Christer Nilsson, C. (2012). Evapotranspiration and crop coefficient for a temperate desert steppe ecosystem using eddy covariance in Inner Mongolia, China. *Hydrological Processes, 26*, 379–386.

Zhang, X., & Zhang, B. (2019). The responses of natural vegetation dynamics to drought during the growing season across China. *Journal of Hydrology, 574*, 706–714.

Zhao, M., Heinsch, F. A., Nemani, R. R., & Running, S. W. (2005). Improving of the MODIS terrestrial gross and net primary production global dataset. *Remote Sensing of Environment, 95*, 164–176.

Zhao, M., & Running, S. W. (2010). Drought-induced reduction in global terrestrial net primary production from 2000 through 2009. *Science, 329*, 940–943.

Zhou, L., & Zhou, G. (2009). Measurement and modeling of evapotranspiration over a reed (Phragmites australis) marsh in Northeast China. *Journal of Hydrology, 372*, 41–47.

Zwart, S. J., Bastiaanssen, W. G. M., De Fraiture, C., & Molden, D. J. (2010). WATPRO: A remote sensing-based model for mapping water productivity of wheat. *Agricultural Water Management, 97*, 1628–1636.